Journal of Computational Physics 230 (2011) 7151–7175

Contents lists available at ScienceDirect

Journal of Computational Physics

journal homepage: www.elsevier.com/locate/jcp

Hybridizable discontinuous Galerkin methods for the time-harmonic Maxwell's equations

N.C. Nguyen [a,*], J. Peraire [a], B. Cockburn [b]

[a] Department of Aeronautics and Astronautics, Massachusetts Institute of Technology, Cambridge, MA 02139, USA
[b] School of Mathematics, University of Minnesota, Minneapolis, MN 55455, USA

ARTICLE INFO

Article history:
Received 24 May 2010
Received in revised form 12 April 2011
Accepted 15 May 2011
Available online 16 June 2011

Keywords:
Finite element method
Discontinuous Galerkin methods
Hybrid/mixed methods
Postprocessing
Maxwell's equations
Computational electromagnetics

ABSTRACT

We present two hybridizable discontinuous Galerkin (HDG) methods for the numerical solution of the time-harmonic Maxwell's equations. The first HDG method explicitly enforces the divergence-free condition and thus necessitates the introduction of a Lagrange multiplier. It produces a linear system for the degrees of freedom of the approximate traces of both the tangential component of the vector field and the Lagrange multiplier. The second HDG method does not explicitly enforce the divergence-free condition and thus results in a linear system for the degrees of freedom of the approximate trace of the tangential component of the vector field only. For both HDG methods, the approximate vector field converges with the optimal order of $k+1$ in the L^2-norm, when polynomials of degree k are used to represent all the approximate variables. We propose elementwise postprocessing to obtain a new $\boldsymbol{H}^{\mathrm{curl}}$-conforming approximate vector field which converges with order $k+1$ in the $\boldsymbol{H}^{\mathrm{curl}}$-norm. We present extensive numerical examples to demonstrate and compare the performance of the HDG methods.

1. Introduction

Computational electromagnetics is of considerable importance in many areas of engineering and science such as aerospace industry, telecommunication, medicine, and biology. Indeed, computational electromagnetics plays a crucial role in the design of novel devices for defense and civil applications. Typical examples of applications include antenna design, the detection of hidden targets, radar, satellite, nanophotonic devices, optical fibers, waveguides, and medical imaging. These applications lead to the development of many computational techniques for solving Maxwell's equations in both frequency and time domains.

The finite element method is a popular computational technique for the solution of electromagnetic problems due to its ability to handle complex geometries and inhomogeneous materials, as well as perform h/p adaptivity. As a class of finite element methods, edge elements [27,28,4,17,18,26] are widely used for numerically solving Maxwell's equations. Edge elements are known to eliminate the problem of spurious modes which may arise when standard finite elements are used to discretize Maxwell's equations [5]. In addition, they can easily handle the boundary conditions and material interface conditions. Low-order edge elements such as the Whitney elements [44] are often used for problems in electromagnetics because they can be easily implemented and avoid the problem of spurious modes. However, the use of low-order edge elements often leads to the discrete system with large numbers of unknowns, especially for electromagnetic problems at high frequencies. As a result, high-order edge elements have been developed [1,2,19,20,41,43] and shown to be more

* Corresponding author. Tel.: +1 617 253 8080.
E-mail address: cuongng@mit.edu (N.C. Nguyen).

0021-9991/$ - see front matter © 2011 Elsevier Inc. All rights reserved.
doi:10.1016/j.jcp.2011.05.018

effective than low-order edge elements. High-order h/p edge elements [19,17,18,24,26,41] perform well for problems with singularities due to reentrant corners and with material interfaces by providing an approximation which converges exponentially when the correct combination of h and p refinements is made. However, high-order edge elements introduce the degrees of freedom in the interior of the elements which increases drastically with the order of approximation [24]. Typically, these interior degrees of freedom can be eliminated by using a procedure known as *static condensation* [24].

Recently, there have been considerable interests in the application of discontinuous Galerkin (DG) methods to computational electromagnetics. In [21,22], the local discontinuous Galerkin (LDG) method with high-order nodal elements is used to solve Maxwell equations on unstructured meshes without explicitly enforcing the divergence-free condition. In [15], the locally divergence-free discontinuous Galerkin method is developed for solving time-dependent Maxwell's equations. For time-dependent Maxwell's equations, with the use of explicit time integration schemes, DG methods [40,42] have the advantage of decoupling all the elements and thus enable parallel efficiency. The LDG method [39] and the interior penalty (IP) method [23] have also been used for solving Maxwell's equations in frequency domain. DG methods have several distinct advantages including their capabilities to handle complex geometries, to provide high-order accurate solutions, to perform h/p adaptivity, and to retain excellent scalability. However, many existing DG methods are known to be computationally expensive because they have too many degrees of freedom due to nodal duplication on the element boundaries [37,38].

In this paper, we introduce hybridizable discontinuous Galerkin (HDG) methods that aim to retain the strengths of DG methods and address the main criticism of DG methods, namely, the excessive number of globally-coupled degrees of freedom. The approach is based upon our recent work on HDG methods [10,12,31,16] for the Stokes system (see also [8,9]), which in turn is an extension of HDG methods for convection–diffusion [11,6,7,29,30]. Recent work includes the development of HDG methods for incompressible flows [33,32,34], for compressible flows [36], and for acoustics and elastodynamics [35].

For scalar diffusion-dominated problems with smooth solutions, these HDG methods provide an optimal convergence of order $k+1$ in the $L^2(\Omega)$-norm for both the approximate solution and its gradient [6,29,30]. They also possess some superconvergence properties that allow us by means of local postprocessing to obtain a new approximation which converges with order $k+2$ in the $L^2(\Omega)$-norm. This has been rigorously proven in [14,13] in the purely diffusive case. It turns out that the HDG methods for the gradient-based formulation of the Stokes flows [12,31] and the incompressible Navier–Stokes equations [32,34] as well as acoustics and elastodynamics [35] possess similar convergence and superconvergence properties. However, the HDG method for the vorticity–velocity–pressure formulation of the Stokes flow [16] does not seem to possess superconvergence, although it does provide an optimal convergence of order $k+1$ for the approximate velocity, pressure, and vorticity.

We present here two HDG methods for the numerical solution of the time-harmonic Maxwell's equations. The first HDG method explicitly enforces the divergence-free condition and thus necessitates the introduction of a Lagrange multiplier. It produces a linear system for the degrees of freedom of the approximate traces of both the tangential component of the vector field and the Lagrange multiplier. The second HDG method does not explicitly enforce the divergence-free condition and thus results in a linear system for the degrees of freedom of the approximate trace of the tangential component of the vector field. For both HDG methods, the approximate vector field converges with the optimal order of $k+1$ in the L^2-norm, when polynomials of degree k are used to represent all the approximate variables. Although the approximate vector field is completely discontinuous across inter element boundaries, we propose an element-by-element postprocessing method to obtain a new approximation whose tangential component is actually continuous, that is, a new approximation which lies in the space $\boldsymbol{H}^{\mathrm{curl}}$-conforming. We show that it converges with order $k+1$ in the $\boldsymbol{H}^{\mathrm{curl}}$-norm. Since the postprocessing is performed at the element level, the computational effort to obtain this new approximate vector field is negligible in comparison with that needed to obtain the original approximate vector field.

Compared to the IP method [23] for the time-harmonic Maxwell's equations, the HDG methods have less globally coupled unknowns. This is not only because the numerical traces are single-valued across the element interfaces, but also because the HDG methods solve for the tangential component of the vector field only. In contrast, the IP method solves for an approximation of the full vector field which has nodal duplication along the inter-element boundaries. For the IP method, the approximate vector field converges with order $k+1$ in the L^2-norm, but with order k in the $\boldsymbol{H}^{\mathrm{curl}}$-norm. Moreover, there is no local postprocessing available for the IP method to increase the convergence rate of the approximate vector field in the $\boldsymbol{H}^{\mathrm{curl}}$-norm.

Let us briefly compare our HDG methods with the high-order edge finite element methods. First, we note that both methods have similar globally-coupled degrees of freedom. The mechanism for reducing the globally-coupled degrees of freedom of the HDG methods is fairly similar to that of edge finite element methods. Indeed, the *hybridization* technique that HDG methods use to achieve this goal, which involves solving local problems at the element level, is essentially a variation of the standard *static condensation* technique that edge finite element methods employ. The former uses weak formulations to directly construct the global matrix whereas the latter works directly with the already assembled matrix. For the h-version of the edge finite element methods, the approximate vector field converges with order k in the $\boldsymbol{H}^{\mathrm{curl}}$-norm when $\boldsymbol{H}^{\mathrm{curl}}$-conforming polynomials of degree k are used to represent the approximate solution [19]. For the HDG methods, local postprocessing is available to yield an improved order of accuracy of $k+1$ in the $\boldsymbol{H}^{\mathrm{curl}}$-norm. This feature can be regarded as the main advantage of the HDG methods over high-order edge finite element methods.

The article is organized as follows. In Section 2, we introduce the notation used throughout the paper. In Section 3, we introduce the HDG method for solving the mixed curl–curl formulation of the time-harmonic Maxwell's equations. In Section

4, we introduce the second HDG method for solving the curl–curl formulation of the time-harmonic Maxwell's equations. In Section 5, we discuss the implementation of the HDG methods for the two-dimensional case. In Section 6, we propose a local postprocessing scheme to obtain an improved $\boldsymbol{H}^{\text{curl}}$-conforming approximation. In Section 7, we present numerical results to assess the performance of the HDG methods. Finally, in Section 8, we provide some concluding remarks.

2. Problem statement and notation

2.1. Maxwell's equations in frequency domain

The Maxwell's equations [19,24] in frequency domain read as follows:

$$\begin{aligned} &\nabla \times \boldsymbol{H} = i\epsilon\omega\boldsymbol{E} + \sigma\boldsymbol{E} + \boldsymbol{J}^s, \\ &\nabla \times \boldsymbol{E} = -i\mu\omega\boldsymbol{H}, \\ &\nabla \cdot \epsilon\boldsymbol{E} = \rho, \\ &\nabla \cdot \mu\boldsymbol{H} = 0. \end{aligned} \tag{1}$$

Here $\boldsymbol{E}$ is the electric field, $\boldsymbol{H}$ is the magnetic field, $\boldsymbol{J}^s$ is the applied current density, ρ is the electric charge density, and ω is the frequency. In addition, ϵ, μ and σ denote the permittivity, permeability and conductivity of the medium, respectively. Note that i denotes the imaginary unit.

In many electromagnetic problems, we can make certain assumptions that greatly simplify the Maxwell's equations. For our purposes here we shall assume that (1) the medium has zero charge density and zero conductivity (namely, $\sigma = 0$ and $\rho = 0$); (2) the applied current density is divergence-free (namely, $\nabla \cdot \boldsymbol{J}^s = 0$); (3) the material properties ϵ and μ depend only on spatial coordinates $\boldsymbol{x}$ and are positive everywhere; and (4) electromagnetic waves propagate in a simply connected and bounded domain $\Omega \in \mathbb{R}^d$ with Lipschitz boundary $\partial\Omega$. Under these assumptions, the time-harmonic Maxwell's equations in the physical domain Ω are as follows:

$$\begin{aligned} &\nabla \times \boldsymbol{H} = i\epsilon\omega\boldsymbol{E} + \boldsymbol{J}^s, \\ &\nabla \times \boldsymbol{E} = -i\mu\omega\boldsymbol{H}, \\ &\nabla \cdot \epsilon\boldsymbol{E} = 0, \\ &\nabla \cdot \mu\boldsymbol{H} = 0. \end{aligned} \tag{2}$$

Note that if we take the divergence of the first two equations we obtain exactly the last two equations of (2). Therefore, the two divergence-free conditions are implicitly present in the first two equations of (2) for $\omega \neq 0$.

The first-order Maxwell's equation (2) can be reduced to a time-harmonic vector wave equation in terms of either the electric field $\boldsymbol{E}$ or the magnetic field $\boldsymbol{H}$. In particular, the first two equations of (2) can be combined to form the time-harmonic vector wave equation in terms of the electric field as

$$\nabla \times (\mu^{-1}\nabla \times \boldsymbol{E}) - \omega^2\epsilon\boldsymbol{E} = -i\omega\boldsymbol{J}^s, \quad \text{in } \Omega. \tag{3}$$

We assume that the vector wave equation is accompanied with the following boundary condition

$$\boldsymbol{n} \times \boldsymbol{E} = \boldsymbol{g}, \quad \text{on } \partial\Omega, \tag{4}$$

where $\boldsymbol{g}$ is a given function on $\partial\Omega$. For the special case $\boldsymbol{g} = \boldsymbol{0}$, the medium is called a *perfect electric conductor*. Of course, we can also derive a vector wave equation in terms of the magnetic field $\boldsymbol{H}$. However, we intend to solve the vector wave Eq. (3) for $\boldsymbol{E}$ and then recover $\boldsymbol{H} = i\mu^{-1}\omega^{-1}\nabla \times \boldsymbol{E}$.

In addition, we are also interested in solving a mixed curl–curl formulation of the time-harmonic Maxwell's equations

$$\begin{aligned} &\nabla \times (\mu^{-1}\nabla \times \boldsymbol{E}) - \omega^2\epsilon\boldsymbol{E} + \epsilon\nabla p = -i\omega\boldsymbol{J}^s, \quad \text{in } \Omega, \\ &\nabla \cdot \epsilon\boldsymbol{E} = 0, \quad \text{in } \Omega, \\ &\boldsymbol{n} \times \boldsymbol{E} = \boldsymbol{g}, \quad \text{on } \partial\Omega, \\ &p = 0, \quad \text{on } \partial\Omega. \end{aligned} \tag{5}$$

Here p is a scalar potential or a Lagrange multiplier introduced to enforce the divergence-free condition explicitly. It can be easily shown that $p = 0$. Indeed, by taking the divergence of the first equation of (5) we obtain that $\nabla \cdot \epsilon\nabla p = 0$ in Ω, which together with $p = 0$ on $\partial\Omega$ implies that $p = 0$ everywhere in the domain. The mixed curl–curl formulation (5) is more stable than the standard vector wave Eq. (3) for problems with small or zero frequency.

2.2. Mesh and trace operators

We denote by $\mathcal{T}_h$ a collection of disjoint regular elements K that partition the domain $\Omega \subset \mathbb{R}$. The set $\partial\mathcal{T}_h := \{\partial K : K \in \mathcal{T}_h\}$ is then a collection of boundaries of the elements. For an element $K \in \mathcal{T}_h, F = \partial K \cap \partial\Omega$ is a boundary face if the $d-1$ Lebesgue measure of F is nonzero. For two elements K^+ and K^- of the collection $\mathcal{T}_h, F = \partial K^+ \cap \partial K^-$ is an interior face between K^+

and K^- if the $d-1$ Lebesgue measure of F is nonzero. We denote by $\mathcal{E}_h^o$ and $\mathcal{E}_h^\partial$ the set of interior and boundary faces, respectively. We set $\mathcal{E}_h = \mathcal{E}_h^o \cup \mathcal{E}_h^\partial$.

Let $\boldsymbol{n}^+$ and $\boldsymbol{n}^-$ be the outward unit normal vectors on two neighboring elements K^+ and K^-, respectively. We use $\boldsymbol{v}^\pm$ to denote the trace of $\boldsymbol{v}$ on F from the interior of $K^\pm$, where $\boldsymbol{v}$ is a function in $\boldsymbol{L}^2(\Omega) \equiv [L^2(\Omega)]^d$. Then, we define the jumps $[\![\cdot]\!]$ as follows. For $F \in \mathcal{E}_h^o$, we set

$$[\![\boldsymbol{v} \odot \boldsymbol{n}]\!] = \boldsymbol{v}^+ \odot \boldsymbol{n}^+ + \boldsymbol{v}^- \odot \boldsymbol{n}^-.$$

Here $\odot$ is either $\cdot$ or $\times$. For $F \in \mathcal{E}_h^\partial$, the set of boundary edges on which $\boldsymbol{v}$ is single valued, we set

$$[\![\boldsymbol{v} \odot \boldsymbol{n}]\!] = \boldsymbol{v} \odot \boldsymbol{n},$$

where $\boldsymbol{n}$ is the unit outward normal to $\partial\Omega$. We further set

$$\boldsymbol{v}^t := \boldsymbol{n} \times (\boldsymbol{v} \times \boldsymbol{n}), \quad \boldsymbol{v}^n := \boldsymbol{n}(\boldsymbol{v} \cdot \boldsymbol{n}),$$

where $\boldsymbol{v}^t$ and $\boldsymbol{v}^n$ represent the tangential and normal components of $\boldsymbol{v}$, respectively. Note that $\boldsymbol{v} = \boldsymbol{v}^t + \boldsymbol{v}^n$.

2.3. Function spaces and approximation spaces

Let D be an open domain in $\mathbb{R}^d$. We recall that $L^2(D)$ is the space of square integrable functions on D and that $H^1(D)$ is the Hilbert space with

$$H^1(D) = \{v \in L^2(D) : \int_D |\nabla v|^2 < \infty\}.$$

We then set $\boldsymbol{L}^2(D) \equiv [L^2(D)]^d$ and define

$$\boldsymbol{H}^{\mathrm{curl}}(D) = \{\boldsymbol{v} \in \boldsymbol{L}^2(D) : \nabla \times \boldsymbol{v} \in [L^2(D)]^n\},$$

where $n = 3$ for $d = 3$ and $n = 1$ for $d = 2$. The $\boldsymbol{H}^{\mathrm{curl}}$-norm associated with this space is defined as

$$\|\boldsymbol{v}\|_{\boldsymbol{H}^{\mathrm{curl}}(D)} = \left(\int_D |\boldsymbol{v}|^2 + |\nabla \times \boldsymbol{v}|^2\right)^{1/2}.$$

We note that the weak formulation of the governing Eq. (5) has a solution $(\boldsymbol{E},p) \in \boldsymbol{H}^{\mathrm{curl}}(\Omega) \times H^1(\Omega)$; see [26].

Let $\mathcal{P}_m(D)$ denote the space of *complex-valued* polynomials of degree at most m on D. We set $\boldsymbol{\mathcal{P}}_m(D) \equiv [\mathcal{P}_m(D)]^d$. We introduce the following approximation spaces

$$P_h = \{q \in L^2(\mathcal{T}_h) : q|_K \in \mathcal{P}_k(K)\ \forall K \in \mathcal{T}_h\},$$
$$\boldsymbol{V}_h = \{\boldsymbol{v} \in \boldsymbol{L}^2(\mathcal{T}_h) : \boldsymbol{v}|_K \in \boldsymbol{\mathcal{P}}_k(K)\ \forall K \in \mathcal{T}_h\}.$$

In addition, we introduce approximation spaces which are defined on $\mathcal{E}_h$ as

$$M_h = \{\zeta \in L^2(\mathcal{E}_h) : \zeta|_F \in \mathcal{P}_k(F)\ \forall F \in \mathcal{E}_h\},$$
$$\boldsymbol{M}_h^t = \{\boldsymbol{\eta} \in \boldsymbol{L}^2(\mathcal{E}_h) : \eta|_F \in \boldsymbol{\mathcal{P}}_k(F), (\boldsymbol{\eta} \cdot \boldsymbol{n})|_F = 0\ \forall F \in \mathcal{E}_h\}.$$

We set $\boldsymbol{M}_h^t(\boldsymbol{g}) = \{\boldsymbol{\eta} \in \boldsymbol{M}_h^t : \boldsymbol{n} \times \boldsymbol{\eta} = \boldsymbol{\Pi g}$ on $\partial\Omega\}$ and $M_h(g) = \{\zeta \in M_h : \zeta = \Pi g$ on $\partial\Omega\}$, where $\boldsymbol{\Pi g}$ (respectively, Πg) denotes a projection of $\boldsymbol{g}$ onto $\boldsymbol{M}_h^t$ (respectively, g onto M_h). Note that $\boldsymbol{M}_h^t$ consists of vector-valued functions whose normal component is zero on any face $F \in \mathcal{E}_h$.

Finally, we define various inner products for our finite element spaces. The volume inner products are defined as

$$(\eta,\zeta)_{\mathcal{T}_h} := \sum_{K \in \mathcal{T}_h} (\eta,\zeta)_K \quad \text{and} \quad (\boldsymbol{\eta},\boldsymbol{\zeta})_{\mathcal{T}_h} := \sum_{i=1}^d (\eta_i,\zeta_i)_{\mathcal{T}_h},$$

where $(\eta, \zeta)_D$ denotes the integral of $\eta\bar{\zeta}$ over the domain $D \subset \mathbb{R}^d$. Here the over-line denotes a complex conjugate. The boundary inner products are defined as

$$\langle \eta,\zeta\rangle_{\partial\mathcal{T}_h} := \sum_{K \in \mathcal{T}_h} \langle \eta,\zeta\rangle_{\partial K} \quad \text{and} \quad \langle \boldsymbol{\eta},\boldsymbol{\zeta}\rangle_{\partial\mathcal{T}_h} := \sum_{i=1}^d \langle \eta_i,\zeta_i\rangle_{\partial\mathcal{T}_h},$$

where $\langle \eta, \zeta\rangle_D$ denotes the integral of $\eta\bar{\zeta}$ over the domain $D \subset \mathbb{R}^{d-1}$. We note that the complex conjugate is applied only to the *second* argument of the inner products.

We are ready to introduce a HDG method for the mixed curl–curl formulation in Section 3 and another HDG method for the vector wave equation in Section 4. We shall pay a greater attention to the HDG method for the mixed curl–curl formulation because this method is more involved than the other one.

3. The mixed curl–curl formulation

3.1. Formulation of the HDG method

We first develop a HDG method for numerically solving the mixed curl–curl formulation (5). We begin by introducing some new variables $\boldsymbol{u} = \boldsymbol{E}$ and $\boldsymbol{w} = \mu^{-1}\nabla\times\boldsymbol{u}$. We can thus rewrite (5) as a first-order system of equations

$$\begin{aligned}
&\mu\boldsymbol{w} - \nabla\times\boldsymbol{u} = 0, \quad \text{in } \Omega,\\
&\nabla\times\boldsymbol{w} - \epsilon\omega^2\boldsymbol{u} + \epsilon\nabla p = \boldsymbol{j}, \quad \text{in } \Omega,\\
&\nabla\cdot\epsilon\boldsymbol{u} = 0, \quad \text{in } \Omega,\\
&\boldsymbol{n}\times\boldsymbol{u} = \boldsymbol{g}, \quad \text{on } \partial\Omega,\\
&p = 0, \quad \text{on } \partial\Omega.
\end{aligned} \tag{6}$$

where $\boldsymbol{j} = -i\omega\boldsymbol{J}^s$ is the new source term. Note that the magnetic field $\boldsymbol{H}$ is related to $\boldsymbol{w}$ by $\boldsymbol{H} = i\omega^{-1}\boldsymbol{w}$.

We seek an approximation $(\boldsymbol{w}_h, \boldsymbol{u}_h, p_h, \hat{\boldsymbol{u}}_h^t, \hat{p}_h) \in \boldsymbol{V}_h\times\boldsymbol{V}_h\times P_h\times\boldsymbol{M}_h^t(\boldsymbol{g})\times M_h(0)$ such that

$$\begin{aligned}
&(\mu\boldsymbol{w}_h, \boldsymbol{r})_{\mathcal{T}_h} - (\boldsymbol{u}_h, \nabla\times\boldsymbol{r})_{\mathcal{T}_h} - \langle\hat{\boldsymbol{u}}_h^t, \boldsymbol{r}\times\boldsymbol{n}\rangle_{\partial\mathcal{T}_h} = 0,\\
&(\boldsymbol{w}_h, \nabla\times\boldsymbol{v})_{\mathcal{T}_h} + \langle\hat{\boldsymbol{w}}_h, \boldsymbol{v}\times\boldsymbol{n}\rangle_{\partial\mathcal{T}_h} - (p_h, \nabla\cdot\epsilon\boldsymbol{v})_{\mathcal{T}_h} + \langle\epsilon\hat{p}_h, \boldsymbol{v}\cdot\boldsymbol{n}\rangle_{\partial\mathcal{T}_h} - (\epsilon\omega^2\boldsymbol{u}_h, \boldsymbol{v})_{\mathcal{T}_h} = (\boldsymbol{j}, \boldsymbol{v})_{\mathcal{T}_h},\\
&-(\epsilon\boldsymbol{u}_h, \nabla q)_{\mathcal{T}_h} + \langle\hat{\boldsymbol{u}}_h^n\cdot\boldsymbol{n}, \epsilon q\rangle_{\partial\mathcal{T}_h} = 0,\\
&-\langle\boldsymbol{n}\times\hat{\boldsymbol{w}}_h, \boldsymbol{\eta}\rangle_{\partial\mathcal{T}_h} = 0,\\
&-\langle\hat{\boldsymbol{u}}_h^n\cdot\boldsymbol{n}, \epsilon\zeta\rangle_{\partial\mathcal{T}_h} = 0,
\end{aligned} \tag{7}$$

for all $(\boldsymbol{r}, \boldsymbol{v}, q, \boldsymbol{\eta}, \zeta) \in \boldsymbol{V}_h\times\boldsymbol{V}_h\times P_h\times\boldsymbol{M}_h^t(\boldsymbol{0})\times M_h(0)$, where

$$\begin{aligned}
&\hat{\boldsymbol{w}}_h = \boldsymbol{w}_h + \tau_t(\boldsymbol{u}_h^t - \hat{\boldsymbol{u}}_h^t)\times\boldsymbol{n},\\
&\hat{\boldsymbol{u}}_h^n = \boldsymbol{u}_h^n + \tau_n(p_h - \hat{p}_h)\boldsymbol{n}.
\end{aligned} \tag{8}$$

Here τ_t and τ_n are *stabilization parameters* which have an important effect on the stability and accuracy of the method. They are chosen based on a dimensional analysis to ensure the same dimensionality for the left and right hand sides of (8). In particular, we choose

$$\tau_t = \sqrt{\frac{\epsilon\omega^2}{\mu}} \quad \text{and} \quad \tau_n = \sqrt{\frac{\epsilon\mu}{\omega^2}}. \tag{9}$$

This completes the definition of the HDG method for the mixed curl–curl formulation.

3.2. Local conservation and consistency

We begin our study of the HDG method under consideration by considering its conservation and consistency properties.

Proposition 1. *The HDG method defined by (7) and (8) is locally conservative and consistent.*

Proof. When ϵ is constant on each face, the last two equations of (7) imply that

$$\begin{aligned}
&[\![\boldsymbol{n}\times\hat{\boldsymbol{w}}_h]\!] = 0, \quad \text{on } \mathcal{E}_h^o,\\
&[\![\boldsymbol{n}\cdot\hat{\boldsymbol{u}}_h^n]\!] = 0, \quad \text{on } \mathcal{E}_h^o.
\end{aligned} \tag{10}$$

Substituting (8) into (10) we obtain

$$\begin{aligned}
&[\![\boldsymbol{n}\times\boldsymbol{w}_h]\!] + \tau_t^+\boldsymbol{u}_h^{t+} + \tau_t^-\boldsymbol{u}_h^{t-} - (\tau_t^+ + \tau_t^-)\hat{\boldsymbol{u}}_h^t = 0, \quad \text{on } \mathcal{E}_h^o,\\
&[\![\boldsymbol{u}_h^n\cdot\boldsymbol{n}]\!] + \tau_n^+p_h^+ + \tau_n^-p_h^- - (\tau_n^+ + \tau_n^-)\hat{p}_h = 0, \quad \text{on } \mathcal{E}_h^o,
\end{aligned}$$

which yields

$$\begin{aligned}
&\hat{\boldsymbol{u}}_h^t = \frac{\tau_t^+\boldsymbol{u}_h^{t+} + \tau_t^-\boldsymbol{u}_h^{t-}}{\tau_t^- + \tau_t^+} + \frac{1}{\tau_t^- + \tau_t^+}[\![\boldsymbol{n}\times\boldsymbol{w}_h]\!], \quad \text{on } \mathcal{E}_h^o,\\
&\hat{p}_h = \frac{\tau_n^+p_h^+ + \tau_n^-p_h^-}{\tau_t^- + \tau_t^+} + \frac{1}{\tau_n^- + \tau_n^+}[\![\boldsymbol{u}_h\cdot\boldsymbol{n}]\!], \quad \text{on } \mathcal{E}_h^o.
\end{aligned} \tag{11}$$

Substituting these expressions into (8) we get

$$\begin{aligned}
&\hat{\boldsymbol{w}}_h = \frac{\tau_t^-\boldsymbol{w}_h^+ + \tau_t^+\boldsymbol{w}_h^-}{\tau_t^- + \tau_t^+} + \frac{\tau_t^-\tau_t^+}{\tau_t^- + \tau_t^+}[\![\boldsymbol{u}_h\times\boldsymbol{n}]\!], \quad \text{on } \mathcal{E}_h^o,\\
&\hat{\boldsymbol{u}}_h^n = \frac{\tau_n^-\boldsymbol{u}_h^{n+} + \tau_n^+\boldsymbol{u}_h^{n-}}{\tau_n^- + \tau_n^+} + \frac{\tau_n^-\tau_n^+}{\tau_n^- + \tau_n^+}[\![p_h\boldsymbol{n}]\!], \quad \text{on } \mathcal{E}_h^o.
\end{aligned} \tag{12}$$

The expressions (11) and (12) show that the numerical traces of the HDG method are single-valued across inter-element boundaries. Therefore, the HDG method is locally conservative according to the definition of local conservation introduced in [3].

Since $u \in H^{\mathrm{curl}}(\Omega)$ and $p \in H^1(\Omega)$, we have $\hat{\boldsymbol{u}}^t = \boldsymbol{u}^t$ and $\hat{p} = p$ on $\mathcal{E}_h$. It thus follows from (8) that $\hat{\boldsymbol{w}} = \boldsymbol{w}$ and $\hat{\boldsymbol{u}}^n = \boldsymbol{u}^n$. Substituting them into the first three equations of (7) and integrating by parts, we obtain

$$\begin{aligned}
&(\mu \boldsymbol{w} - \nabla \times \boldsymbol{u}, \boldsymbol{r})_{\mathcal{T}_h} = 0, \quad \forall \boldsymbol{r} \in \boldsymbol{W}_h,\\
&(\nabla \times \boldsymbol{w} - \epsilon\omega^2 \boldsymbol{u} + \epsilon \nabla p, \boldsymbol{v})_{\mathcal{T}_h} = (\boldsymbol{j}, \boldsymbol{v})_{\mathcal{T}_h}, \quad \forall \boldsymbol{v} \in \boldsymbol{V}_h,\\
&(\nabla \cdot \epsilon \boldsymbol{u}, q)_{\mathcal{T}_h} = 0, \quad \forall q \ \in P_h.
\end{aligned} \tag{13}$$

This implies that the exact solution of (5) satisfies the HDG formulation (7) and (8). Hence, the HDG method is consistent. This completes the proof. □

3.3. Existence and uniqueness

Moreover, we can show that the HDG method is well defined.

Proposition 2. *Assume that $\epsilon\omega^2$ is different from the eigenvalue λ of the following eigenproblem: find $\lambda \in \mathbb{R}$ and $(\boldsymbol{s}_h, \boldsymbol{z}_h, \psi_h, \hat{\boldsymbol{z}}_h^t, \hat{\psi}_h) \in \boldsymbol{V}_h \times \boldsymbol{V}_h \times P_h \times \boldsymbol{M}_h^t(\boldsymbol{0}) \times M_h(0)$ such that*

$$\begin{aligned}
&(\mu \boldsymbol{s}_h, \boldsymbol{r})_{\mathcal{T}_h} - (\boldsymbol{z}_h, \nabla \times \boldsymbol{r})_{\mathcal{T}_h} - \langle \hat{\boldsymbol{z}}_h^t, \boldsymbol{r} \times \boldsymbol{n} \rangle_{\partial\mathcal{T}_h} = 0,\\
&(\boldsymbol{s}_h, \nabla \times \boldsymbol{v})_{\mathcal{T}_h} + \langle \hat{\boldsymbol{s}}_h, \boldsymbol{v} \times \boldsymbol{n} \rangle_{\partial\mathcal{T}_h} - (\psi_h, \nabla \cdot \epsilon \boldsymbol{v})_{\mathcal{T}_h} + \langle \epsilon \hat{\psi}_h, \boldsymbol{v} \cdot \boldsymbol{n} \rangle_{\partial\mathcal{T}_h} = \lambda (\boldsymbol{z}_h, \boldsymbol{v})_{\mathcal{T}_h},\\
&-(\epsilon \boldsymbol{z}_h, \nabla q)_{\mathcal{T}_h} + \langle \hat{\boldsymbol{z}}_h^n \cdot \boldsymbol{n}, \epsilon q \rangle_{\partial\mathcal{T}_h} = 0,\\
&-\langle \boldsymbol{n} \times \hat{\boldsymbol{s}}_h, \boldsymbol{\eta} \rangle_{\partial\mathcal{T}_h} = 0,\\
&-\langle \hat{\boldsymbol{z}}_h^n \cdot \boldsymbol{n}, \epsilon \zeta \rangle_{\partial\mathcal{T}_h} = 0,
\end{aligned} \tag{14}$$

for all $(\boldsymbol{r}, \boldsymbol{v}, q, \boldsymbol{\eta}^t, \zeta) \in \boldsymbol{W}_h \times \boldsymbol{V}_h \times P_h, \times \boldsymbol{M}_h^t(\boldsymbol{0}) \times M_h(0)$, where

$$\begin{aligned}
\hat{\boldsymbol{s}}_h &= \boldsymbol{s}_h + \tau_t (\boldsymbol{z}_h^t - \hat{\boldsymbol{z}}_h^t) \times \boldsymbol{n},\\
\hat{\boldsymbol{z}}_h^n &= \boldsymbol{z}_h^n + \tau_n (\psi_h - \hat{\psi}_h) \boldsymbol{n}.
\end{aligned} \tag{15}$$

Moreover, we assume that the stabilization parameters τ_t and τ_n satisfy the condition

$$\tau_t > 0 \quad \text{and} \quad \tau_n > 0 \quad \text{on } \partial\mathcal{T}_h. \tag{16}$$

Then the HDG solution $(\boldsymbol{w}_h, \boldsymbol{u}_h, p_h, \hat{\boldsymbol{u}}_h^t, \hat{p}_h)$ exists and is unique.

Proof. Substituting (8) into (7) and integrating by parts we obtain

$$\begin{aligned}
&(\mu \boldsymbol{w}_h, \boldsymbol{r})_{\mathcal{T}_h} - (\boldsymbol{u}_h, \nabla \times \boldsymbol{r})_{\mathcal{T}_h} - \langle \hat{\boldsymbol{u}}_h^t, \boldsymbol{r} \times \boldsymbol{n} \rangle_{\partial\mathcal{T}_h} = 0,\\
&(\nabla \times \boldsymbol{w}_h, \boldsymbol{v})_{\mathcal{T}_h} + \langle \tau_t (\boldsymbol{u}_h^t - \hat{\boldsymbol{u}}_h^t), \boldsymbol{n} \times \boldsymbol{v} \times \boldsymbol{n} \rangle_{\partial\mathcal{T}_h} - (p_h, \nabla \cdot \epsilon \boldsymbol{v})_{\mathcal{T}_h} + \langle \epsilon \hat{p}_h, \boldsymbol{v} \cdot \boldsymbol{n} \rangle_{\partial\mathcal{T}_h} - (\epsilon\omega^2 \boldsymbol{u}_h, \boldsymbol{v})_{\mathcal{T}_h} = (\boldsymbol{j}, \boldsymbol{v})_{\mathcal{T}_h},\\
&(\nabla \cdot \epsilon \boldsymbol{u}_h, q)_{\mathcal{T}_h} + \langle \epsilon \tau_n (p_h - \hat{p}_h), q \rangle_{\partial\mathcal{T}_h} = 0,\\
&-\langle \boldsymbol{n} \times \boldsymbol{w}_h + \tau_t (\boldsymbol{u}_h^t - \hat{\boldsymbol{u}}_h^t), \boldsymbol{\eta}^t \rangle_{\partial\mathcal{T}_h} = 0,\\
&-\langle \boldsymbol{u}_h^n \cdot \boldsymbol{n} + \tau_n (p_h - \hat{p}_h), \epsilon \zeta \rangle_{\partial\mathcal{T}_h} = 0,
\end{aligned} \tag{17}$$

for all $(\boldsymbol{r}, \boldsymbol{v}, q, \boldsymbol{\eta}^t, \zeta) \in \boldsymbol{W}_h \times \boldsymbol{V}_h \times P_h, \times \boldsymbol{M}_h^t(\boldsymbol{0}) \times M_h(0)$. Due to the linearity, finite dimensionality, and to the fact that this is a square system, it is sufficient to show that the only solution of the above system for $j = 0$ and $g = 0$ is $(\boldsymbol{w}_h, \boldsymbol{u}_h, p_h, \hat{\boldsymbol{u}}_h^t, \hat{p}_h) = (0, 0, 0, 0, 0)$.

Indeed, taking $\boldsymbol{r} = \boldsymbol{w}_h, \boldsymbol{v} = \boldsymbol{u}_h, q = p_h, \boldsymbol{\eta}^t = \hat{\boldsymbol{u}}_h^t$, and $\zeta = \hat{p}_h$, and adding the resulting equations all together, we get

$$(\mu \boldsymbol{w}_h, \boldsymbol{w}_h)_{\mathcal{T}_h} + \langle \tau_t (\boldsymbol{u}_h^t - \hat{\boldsymbol{u}}_h^t), (\boldsymbol{u}_h^t - \hat{\boldsymbol{u}}_h^t) \rangle_{\partial\mathcal{T}_h} + \langle \epsilon \tau_n (p_h - \hat{p}_h), (p_h - \hat{p}_h) \rangle_{\partial\mathcal{T}_h} - (\epsilon\omega^2 \boldsymbol{u}_h, \boldsymbol{u}_h)_{\mathcal{T}_h} = 0. \tag{18}$$

Similarly, we have

$$(\mu \boldsymbol{s}_h, \boldsymbol{s}_h)_{\mathcal{T}_h} + \langle \tau_t (\boldsymbol{z}_h^t - \hat{\boldsymbol{z}}_h^t), (\boldsymbol{z}_h^t - \hat{\boldsymbol{z}}_h^t) \rangle_{\partial\mathcal{T}_h} + \langle \epsilon \tau_n (\psi_h - \hat{\psi}_h), (\psi_h - \hat{\psi}_h) \rangle_{\partial\mathcal{T}_h} = \lambda (\boldsymbol{z}_h, \boldsymbol{z}_h)_{\mathcal{T}_h}. \tag{19}$$

It follows from (18) and (19) that $u_h = 0$; otherwise, if $u_h \neq 0$, then $\epsilon\omega^2$ must be an eigenvalue of (14) which contradicts with our assumption $\epsilon\omega^2 \neq \lambda$. As a consequence, we obtain

$$(\mu \boldsymbol{w}_h, \boldsymbol{w}_h)_{\mathcal{T}_h} + \langle \tau_t \hat{\boldsymbol{u}}_h^t, \hat{\boldsymbol{u}}_h^t \rangle_{\partial\mathcal{T}_h} + \langle \epsilon \tau_n (p_h - \hat{p}_h), (p_h - \hat{p}_h) \rangle_{\partial\mathcal{T}_h} = 0, \tag{20}$$

which implies $\boldsymbol{w}_h = 0, \hat{\boldsymbol{u}}_h^t = 0$, and $p_h = \hat{p}_h$ on $\mathcal{T}_h$ since τ_t and τ_n are strictly positive. It then follows from the second equation of (17) that

$$(\epsilon \nabla p_h, \boldsymbol{v})_{\mathcal{T}_h} = 0, \quad \forall\ \boldsymbol{v} \in \boldsymbol{V}_h, \tag{21}$$

which implies that p_h is a constant function. Since $p_h = \hat{p}_h = 0$ on $\partial\Omega$, we have $p_h = 0$ everywhere. This completes the proof. □

3.4. Hybridization of the HDG method

The primary motivation for the hybridization is the reduction in the number of globally-coupled degrees of freedom. This is achieved by locally eliminating the degrees of freedom of the approximate solution to obtain a matrix system involving the degrees of freedom of the approximate trace. The hybridization procedure is thus similar to static condensation. However, unlike the classical approach, hybridization is systematic in the sense that it explicitly yields a weak formulation in terms of the approximate trace.

We begin by noting that the first three equations of (7) can be written as

$$\begin{aligned}
&(\mu \boldsymbol{w}_h, \boldsymbol{r})_K - (\boldsymbol{u}_h, \nabla \times \boldsymbol{r})_K = \langle \hat{\boldsymbol{u}}_h^t, \boldsymbol{r} \times \boldsymbol{n} \rangle_{\partial K}, \\
&(\nabla \times \boldsymbol{w}_h, \boldsymbol{v})_K + \langle \tau_t \boldsymbol{u}_h \times \boldsymbol{n}, \boldsymbol{v} \times \boldsymbol{n} \rangle_{\partial K} - (p_h, \nabla \cdot \epsilon \boldsymbol{v})_K - (\epsilon \omega^2 \boldsymbol{u}_h, \boldsymbol{v})_K = (\boldsymbol{j}, \boldsymbol{v})_K - \langle \epsilon \hat{p}_h, \boldsymbol{v} \cdot \boldsymbol{n} \rangle_{\partial K} + \langle \tau_t \hat{\boldsymbol{u}}_h^t \times \boldsymbol{n}, \boldsymbol{v} \times \boldsymbol{n} \rangle_{\partial K}, \\
&(\nabla \cdot \epsilon \boldsymbol{u}_h, q)_K + \langle \tau_n p_h, \epsilon q \rangle_{\partial K} = \langle \tau_n \hat{p}_h, \epsilon q \rangle_{\partial K},
\end{aligned} \tag{22}$$

for all $(\boldsymbol{r}, \boldsymbol{v}, q) \in \mathcal{P}_k(K) \times \mathcal{P}_k(K) \times P_k(K)$ and all $K \in \mathcal{T}_h$. It is important to note that if $(\hat{\boldsymbol{u}}_h^t, \hat{p}_h, \boldsymbol{j})$ is available, we can compute $(\boldsymbol{w}_h, \boldsymbol{u}_h, p_h)$ in an element-by-element fashion by solving (22) for each $K \in \mathcal{T}_h$. Therefore, (22) defines a "local solver" that maps $(\hat{\boldsymbol{u}}_h^t, \hat{p}_h, \boldsymbol{j})$ to $(\boldsymbol{w}_h, \boldsymbol{u}_h, p_h)$ as

$$(\hat{\boldsymbol{u}}_h^t, \hat{p}_h, \boldsymbol{j}) \overset{\mathcal{L}}{\mapsto} (\boldsymbol{w}_h, \boldsymbol{u}_h, p_h). \tag{23}$$

Since the source term $\boldsymbol{j}$ is known, we only need to determine $(\hat{\boldsymbol{u}}_h^t, \hat{p}_h)$ as follows.

Next, for any given pair of functions $(\xi, \varrho) \in \boldsymbol{M}_h^t \times M_h$ we introduce the following local solutions

$$\begin{aligned}
&(\boldsymbol{w}_h^\xi, \boldsymbol{u}_h^\xi, p_h^\xi) := \mathcal{L}(\boldsymbol{\eta}, 0, 0), \\
&(\boldsymbol{w}_h^\varrho, \boldsymbol{u}_h^\varrho, p_h^\varrho) := \mathcal{L}(0, \varrho, 0), \\
&\left(\boldsymbol{w}_h^{\boldsymbol{j}}, \boldsymbol{u}_h^{\boldsymbol{j}}, p_h^{\boldsymbol{j}}\right) := \mathcal{L}(0, 0, \boldsymbol{j}),
\end{aligned} \tag{24}$$

where $(\boldsymbol{w}_h^\xi, \boldsymbol{u}_h^\xi, p_h^\xi)$, $(\boldsymbol{w}_h^\varrho, \boldsymbol{u}_h^\varrho, p_h^\varrho)$, and $\left(\boldsymbol{w}_h^{\boldsymbol{j}}, \boldsymbol{u}_h^{\boldsymbol{j}}, p_h^{\boldsymbol{j}}\right)$ are obtained from (22) when we replace $(\hat{\boldsymbol{u}}_h^t, \hat{p}_h, \boldsymbol{j})$ with $(\xi, 0, 0)$, $(0, \varrho, 0)$, and $(0, 0, \boldsymbol{j})$, respectively.

The following result is a direct consequence of the decomposition (24) and the last two equations of the HDG system (7).

Lemma 3.1. *Let $(\boldsymbol{w}_h, \boldsymbol{u}_h, p_h, \hat{\boldsymbol{u}}_h^t, \hat{p}_h)$ be the solution of the second HDG formulation (7). We have that*

$$\begin{aligned}
&\boldsymbol{w}_h = \boldsymbol{w}_h^\lambda + \boldsymbol{w}_h^\rho + \boldsymbol{w}_h^{\boldsymbol{j}}, \\
&\boldsymbol{u}_h = \boldsymbol{u}_h^\lambda + \boldsymbol{u}_h^\rho + \boldsymbol{u}_h^{\boldsymbol{j}}, \\
&p_h = p_h^\lambda + p_h^\rho + p_h^{\boldsymbol{j}}, \\
&\hat{\boldsymbol{u}}_h^t = \boldsymbol{\lambda}, \\
&\hat{p}_h = \rho,
\end{aligned} \tag{25}$$

where $(\boldsymbol{\lambda}, \rho) \in \boldsymbol{M}_h^t(\boldsymbol{g}) \times M_h(0)$ is the solution of

$$\begin{aligned}
&a_h(\boldsymbol{\lambda}, \boldsymbol{\eta}) + b_h(\rho, \boldsymbol{\eta}) = \ell_h(\boldsymbol{\eta}), \quad \forall \boldsymbol{\eta} \in \boldsymbol{M}_h^t(\boldsymbol{0}), \\
&d_h(\boldsymbol{\lambda}, \zeta) + c_h(\rho, \zeta) = f_h(\zeta), \quad \forall \zeta \in M_h(0).
\end{aligned} \tag{26}$$

Here the forms are given by

$$\begin{aligned}
&a_h(\xi, \boldsymbol{\eta}) = -\left\langle \boldsymbol{n} \times \boldsymbol{w}_h^\xi + \tau_t \left((\boldsymbol{u}_h^t)^\xi - \xi \right), \boldsymbol{\eta} \right\rangle_{\partial \mathcal{T}_h}, \\
&b_h(\varrho, \boldsymbol{\eta}) = -\left\langle \boldsymbol{n} \times \boldsymbol{w}_h^\varrho + \tau_t (\boldsymbol{u}_h^t)^\varrho, \boldsymbol{\eta} \right\rangle_{\partial \mathcal{T}_h}, \\
&c_h(\varrho, \zeta) = -\left\langle (\boldsymbol{u}_h^n)^\varrho \cdot \boldsymbol{n} + \tau_n (p_h^\varrho - \varrho), \epsilon \zeta \right\rangle_{\partial \mathcal{T}_h}, \\
&d_h(\xi, \zeta) = -\left\langle (\boldsymbol{u}_h^n)^\xi \cdot \boldsymbol{n} + \tau_n p_h^\xi, \epsilon \zeta \right\rangle_{\partial \mathcal{T}_h}, \\
&\ell_h(\boldsymbol{\eta}) = \left\langle \boldsymbol{n} \times \boldsymbol{w}_h^{\boldsymbol{j}} + \tau_t (\boldsymbol{u}_h^t)^{\boldsymbol{j}}, \boldsymbol{\eta} \right\rangle_{\partial \mathcal{T}_h}, \\
&f_h(\zeta) = \left\langle (\boldsymbol{u}_h^n)^{\boldsymbol{j}} \cdot \boldsymbol{n} + \tau_n p_h^{\boldsymbol{j}}, \epsilon \zeta \right\rangle_{\partial \mathcal{T}_h},
\end{aligned} \tag{27}$$

for all $\boldsymbol{\xi},\boldsymbol{\eta}\in\boldsymbol{M}_h^t$ *and* $\varrho,\zeta\in M_h$.

Furthermore, we can establish the following identities whose proof is given in Appendix A.

Lemma 3.2. *We have that*

$$\begin{aligned}
&-\left\langle \boldsymbol{n}\times\boldsymbol{w}_h^{\boldsymbol{\xi}}+\tau_t\left((\boldsymbol{u}_h^t)^{\boldsymbol{\xi}}-\boldsymbol{\xi}\right),\boldsymbol{\eta}\right\rangle_{\partial\mathcal{T}_h}=(\mu\boldsymbol{w}_h^{\boldsymbol{\xi}},\boldsymbol{w}_h^{\boldsymbol{\eta}})_{\mathcal{T}_h}-(\epsilon\omega^2\boldsymbol{u}_h^{\boldsymbol{\xi}},\boldsymbol{u}_h^{\boldsymbol{\eta}})_{\mathcal{T}_h}\\
&\qquad\qquad+\left\langle\tau_t\left((\boldsymbol{u}_h^t)^{\boldsymbol{\xi}}-\boldsymbol{\xi}\right),\left((\boldsymbol{u}_h^t)^{\boldsymbol{\eta}}-\boldsymbol{\eta}\right)\right\rangle_{\partial\mathcal{T}_h}+\langle\tau_n\epsilon p_h^{\boldsymbol{\xi}},p_h^{\boldsymbol{\eta}}\rangle_{\partial\mathcal{T}_h},\\
&-\langle\boldsymbol{n}\times\boldsymbol{w}_h^{\varrho}+\tau_t(\boldsymbol{u}_h^t)^{\varrho},\boldsymbol{\eta}\rangle_{\partial\mathcal{T}_h}=\langle\tau_n p_h^{\boldsymbol{\eta}},\epsilon\varrho\rangle_{\partial\mathcal{T}_h}+\left\langle\epsilon\varrho,(\boldsymbol{u}_h^n)^{\boldsymbol{\eta}}\cdot\boldsymbol{n}\right\rangle_{\partial\mathcal{T}_h},\\
&-\left\langle\boldsymbol{n}\times\boldsymbol{w}_h^{\boldsymbol{j}}+\tau_t(\boldsymbol{u}_h^t)^{\boldsymbol{j}},\boldsymbol{\eta}\right\rangle_{\partial\mathcal{T}_h}=-(\boldsymbol{j},\boldsymbol{u}_h^{\boldsymbol{\eta}})_{\mathcal{T}_h},
\end{aligned}\tag{28}$$

and

$$\begin{aligned}
&-\left\langle(\boldsymbol{u}_h^n)^{\boldsymbol{\xi}}\cdot\boldsymbol{n}+\tau_n p_h^{\boldsymbol{\xi}},\epsilon\zeta\right\rangle_{\partial\mathcal{T}_h}=-\langle\tau_n p_h^{\boldsymbol{\xi}},\epsilon\zeta\rangle_{\partial\mathcal{T}_h}-\left\langle\epsilon\zeta,(\boldsymbol{u}_h^n)^{\boldsymbol{\xi}}\cdot\boldsymbol{n}\right\rangle_{\partial\mathcal{T}_h},\\
&-\left\langle(\boldsymbol{u}_h^n)^{\varrho}\cdot\boldsymbol{n}+\tau_n(p_h^{\varrho}-\varrho),\epsilon\zeta\right\rangle_{\partial\mathcal{T}_h}=(\mu\boldsymbol{w}_h^{\varrho},\boldsymbol{w}_h^{\zeta})_{\mathcal{T}_h}-(\epsilon\omega^2\boldsymbol{u}_h^{\varrho},\boldsymbol{u}_h^{\zeta})_{\mathcal{T}_h}\\
&\qquad\qquad+\langle\tau_n\epsilon(p_h^{\varrho}-\varrho),(p_h^{\zeta}-\zeta)\rangle_{\partial\mathcal{T}_h}+\left\langle\tau_t(\boldsymbol{u}_h^t)^{\varrho},(\boldsymbol{u}_h^t)^{\zeta}\right\rangle_{\partial\mathcal{T}_h},\\
&-\left\langle(\boldsymbol{u}_h^n)^{\boldsymbol{j}}\cdot\boldsymbol{n}+\tau_n p_h^{\boldsymbol{j}},\epsilon\zeta\right\rangle_{\partial\mathcal{T}_h}=(\boldsymbol{j},\boldsymbol{u}_h^{\zeta})_{\mathcal{T}_h},
\end{aligned}\tag{29}$$

for all $\boldsymbol{\xi},\boldsymbol{\eta}\in\boldsymbol{M}_h^t$ *and* $\varrho,\zeta\in M_h$.

As a consequence of Lemmas 3.1 and 3.2, we obtain the following result

Proposition 3. $(\boldsymbol{\lambda},\rho)\in\boldsymbol{M}_h^t(\boldsymbol{g})\times M_h(0)$ *satisfies the following weak formulation*

$$\begin{aligned}
&a_h(\boldsymbol{\lambda},\boldsymbol{\eta})+b_h(\rho,\boldsymbol{\eta})=\ell_h(\boldsymbol{\eta}),\quad\forall\boldsymbol{\eta}\in\boldsymbol{M}_h^t(\boldsymbol{0}),\\
&-b_h(\zeta,\boldsymbol{\lambda})+c_h(\rho,\zeta)=f_h(\zeta),\quad\forall\zeta\in M_h(0).
\end{aligned}\tag{30}$$

Here the forms are given by

$$\begin{aligned}
a_h(\boldsymbol{\xi},\boldsymbol{\eta})&=(\mu\boldsymbol{w}_h^{\boldsymbol{\xi}},\boldsymbol{w}_h^{\boldsymbol{\eta}})_{\mathcal{T}_h}-(\epsilon\omega^2\boldsymbol{u}_h^{\boldsymbol{\xi}},\boldsymbol{u}_h^{\boldsymbol{\eta}})_{\mathcal{T}_h}+\langle\tau_n\epsilon p_h^{\boldsymbol{\xi}},p_h^{\boldsymbol{\eta}}\rangle_{\partial\mathcal{T}_h}+\left\langle\tau_t\left((\boldsymbol{u}_h^t)^{\boldsymbol{\xi}}-\boldsymbol{\xi}\right),\left((\boldsymbol{u}_h^t)^{\boldsymbol{\eta}}-\boldsymbol{\eta}\right)\right\rangle_{\partial\mathcal{T}_h},\\
b_h(\varrho,\boldsymbol{\eta})&=\langle\tau_n p_h^{\boldsymbol{\eta}},\epsilon\varrho\rangle_{\partial\mathcal{T}_h}+\left\langle\epsilon\varrho,(\boldsymbol{u}_h^n)^{\boldsymbol{\eta}}\cdot\boldsymbol{n}\right\rangle_{\partial\mathcal{T}_h},\\
c_h(\varrho,\zeta)&=(\mu\boldsymbol{w}_h^{\varrho},\boldsymbol{w}_h^{\zeta})_{\mathcal{T}_h}-(\epsilon\omega^2\boldsymbol{u}_h^{\varrho},\boldsymbol{u}_h^{\zeta})_{\mathcal{T}_h}+\left\langle\tau_t(\boldsymbol{u}_h^t)^{\varrho},(\boldsymbol{u}_h^t)^{\zeta}\right\rangle_{\partial\mathcal{T}_h}\\
&\quad+\langle\tau_n\epsilon(p_h^{\varrho}-\varrho),(p_h^{\zeta}-\zeta)\rangle_{\partial\mathcal{T}_h},\\
\ell_h(\boldsymbol{\eta})&=(\boldsymbol{j},\boldsymbol{u}_h^{\boldsymbol{\eta}})_{\mathcal{T}_h},\\
f_h(\zeta)&=-(\boldsymbol{j},\boldsymbol{u}_h^{\zeta})_{\mathcal{T}_h},
\end{aligned}\tag{31}$$

for all $\boldsymbol{\xi},\boldsymbol{\eta}\in\boldsymbol{M}_h^t$ *and* $\varrho,\zeta\in M_h$.

We note that (30) is equivalent to (26). However, the weak formulation (30) explicitly shows that the bilinear forms a_h and c_h are symmetric and that the associated matrix system is given by

$$\begin{pmatrix}A & B\\ -B^T & C\end{pmatrix}\begin{pmatrix}\Lambda\\ \Phi\end{pmatrix}=\begin{pmatrix}L\\ F\end{pmatrix},\tag{32}$$

where Λ and Φ represent the vector of degrees of freedom of $\boldsymbol{\lambda}$ and ρ, respectively. Both the weak formulations characterize the solution of the HDG method (7) in terms of $\boldsymbol{\lambda}$ and ρ. Since $\boldsymbol{\lambda}$ and ρ are defined on and single-valued across inter-element boundaries, the HDG method may have less the globally coupled degrees of freedom than other DG methods. This advantage comes with an additional cost of solving the local problems on all elements of the triangulation. However, this additional cost is typically much smaller than the cost of solving the global matrix system (32).

4. The vector wave equation

4.1. Formulation of the HDG method

We now describe a HDG method for solving the vector wave Eq. (3). We begin by writing (3) as a first-order system of equations as

$$\begin{aligned}
&\mu \boldsymbol{w} - \nabla \times \boldsymbol{u} = 0, \quad \text{in } \Omega,\\
&\nabla \times \boldsymbol{w} - \epsilon\omega^2 \boldsymbol{u} = \boldsymbol{j}, \quad \text{in } \Omega,\\
&\boldsymbol{n} \times \boldsymbol{u} = \boldsymbol{g}, \quad \text{on } \partial\Omega,
\end{aligned} \tag{33}$$

where $\boldsymbol{u} = \boldsymbol{E}$, $\boldsymbol{w} = \mu^{-1}\nabla \times \boldsymbol{u}$, and $\boldsymbol{j} = -i\omega \boldsymbol{J}^s$ are the new variables.

The HDG method for the above system then seeks $(\boldsymbol{w}_h, \boldsymbol{u}_h, \hat{\boldsymbol{u}}_h^t) \in \boldsymbol{V}_h \times \boldsymbol{V}_h \times \boldsymbol{M}_h^t(\boldsymbol{g})$ such that

$$\begin{aligned}
&(\mu \boldsymbol{w}_h, \boldsymbol{r})_{\mathcal{T}_h} - (\boldsymbol{u}_h, \nabla \times \boldsymbol{r})_{\mathcal{T}_h} - \langle \hat{\boldsymbol{u}}_h^t, \boldsymbol{r} \times \boldsymbol{n} \rangle_{\partial\mathcal{T}_h} = 0,\\
&(\boldsymbol{w}_h, \nabla \times \boldsymbol{v})_{\mathcal{T}_h} + \langle \hat{\boldsymbol{w}}_h, \boldsymbol{v} \times \boldsymbol{n} \rangle_{\partial\mathcal{T}_h} - (\epsilon\omega^2 \boldsymbol{u}_h, \boldsymbol{v})_{\mathcal{T}_h} = (\boldsymbol{j}, \boldsymbol{v})_{\mathcal{T}_h},\\
&- \langle \boldsymbol{n} \times \hat{\boldsymbol{w}}_h, \boldsymbol{\eta} \rangle_{\partial\mathcal{T}_h} = 0,
\end{aligned} \tag{34}$$

for all $(\boldsymbol{r}, \boldsymbol{v}, \boldsymbol{\eta}) \in \boldsymbol{V}_h \times \boldsymbol{V}_h \times \boldsymbol{M}_h^t(\boldsymbol{0})$, where

$$\hat{\boldsymbol{w}}_h = \boldsymbol{w}_h + \tau(\boldsymbol{u}_h^t - \hat{\boldsymbol{u}}_h^t) \times \boldsymbol{n}. \tag{35}$$

Here the stabilization parameter τ is chosen as

$$\tau = \sqrt{\frac{\epsilon\omega^2}{\mu}}. \tag{36}$$

This completes the definition of the HDG method for the vector wave equation.

Let us briefly comment on the equations defining the HDG method. The first two equations are obtained by multiplying the first two equations in (33) by test functions and integrating by parts. The last equation enforces the continuity of the tangential component of $\hat{\boldsymbol{w}}_h$ across inter-element boundaries, namely,

$$[\![\boldsymbol{n} \times \hat{\boldsymbol{w}}_h]\!] = 0, \quad \text{on } \mathcal{E}_h^o. \tag{37}$$

Finally, we note that $\hat{\boldsymbol{u}}_h^t$ is single-valued across inter-element boundaries and satisfies the boundary condition since $\hat{\boldsymbol{u}}_h^t$ belongs to $\boldsymbol{M}_h^t(\boldsymbol{g})$.

4.2. Local conservation

We now derive explicit expressions of the approximate traces in terms of the approximate solution. To this end we insert (35) into (37) to obtain

$$[\![\boldsymbol{n} \times \boldsymbol{w}_h]\!] + \tau^+ \boldsymbol{u}_h^{t+} + \tau^- \boldsymbol{u}_h^{t-} - (\tau^+ + \tau^-)\hat{\boldsymbol{u}}_h^t = 0, \quad \text{on } \mathcal{E}_h^o,$$

which yields

$$\hat{\boldsymbol{u}}_h^t = \frac{\tau^+ \boldsymbol{u}_h^{t+} + \tau^- \boldsymbol{u}_h^{t-}}{\tau^- + \tau^+} + \frac{1}{\tau^- + \tau^+}[\![\boldsymbol{n} \times \boldsymbol{w}_h]\!], \quad \text{on } \mathcal{E}_h^o. \tag{38}$$

Substituting (38) into (35) we get

$$\hat{\boldsymbol{w}}_h = \frac{\tau^- \boldsymbol{w}_h^+ + \tau^+ \boldsymbol{w}_h^-}{\tau^- + \tau^+} + \frac{\tau^- \tau^+}{\tau^- + \tau^+}[\![\boldsymbol{u}_h \times \boldsymbol{n}]\!], \quad \text{on } \mathcal{E}_h^o. \tag{39}$$

This expression shows that the HDG method (34) is locally conservative because $\hat{\boldsymbol{w}}_h$ is single-valued across inter-element boundaries.

Furthermore, the HDG method can be viewed in a more traditional way as a DG method that finds $(\boldsymbol{w}_h, \boldsymbol{u}_h) \in \boldsymbol{V}_h \times \boldsymbol{V}_h$ such that

$$\begin{aligned}
&(\mu \boldsymbol{w}_h, \boldsymbol{r})_{\mathcal{T}_h} - (\boldsymbol{u}_h, \nabla \times \boldsymbol{r})_{\mathcal{T}_h} - \langle \hat{\boldsymbol{u}}_h^t, \boldsymbol{r} \times \boldsymbol{n} \rangle_{\partial\mathcal{T}_h} = 0,\\
&(\boldsymbol{w}_h, \nabla \times \boldsymbol{v})_{\mathcal{T}_h} + \langle \hat{\boldsymbol{w}}_h, \boldsymbol{v} \times \boldsymbol{n} \rangle_{\partial\mathcal{T}_h} - (\epsilon\omega^2 \boldsymbol{u}_h, \boldsymbol{v})_{\mathcal{T}_h} = (\boldsymbol{j}, \boldsymbol{v})_{\mathcal{T}_h},
\end{aligned} \tag{40}$$

for all $(\boldsymbol{r}, \boldsymbol{v}) \in \boldsymbol{V}_h \times \boldsymbol{V}_h$. Here the numerical traces $\hat{\boldsymbol{u}}_h^t$ and $\hat{\boldsymbol{w}}_h$ are defined by (38) and (39), respectively.

4.3. Hybridization of the HDG method

Let us turn our attention to the hybridization of the HDG method (34). To this end, we introduce two local solvers. The first local solver maps $\boldsymbol{\eta} \in \boldsymbol{M}_h^t$ to $(\boldsymbol{w}_h^{\boldsymbol{\eta}}, \boldsymbol{u}_h^{\boldsymbol{\eta}}) \in \mathcal{P}_k(K) \times \mathcal{P}_k(K)$ such that

$$\begin{aligned}
&(\mu \boldsymbol{w}_h^{\boldsymbol{\eta}}, \boldsymbol{r})_K - (\boldsymbol{u}_h^{\boldsymbol{\eta}}, \nabla \times \boldsymbol{r})_K = \langle \boldsymbol{\eta}, \boldsymbol{r} \times \boldsymbol{n} \rangle_{\partial K},\\
&(\nabla \times \boldsymbol{w}_h^{\boldsymbol{\eta}} - \epsilon\omega^2 \boldsymbol{u}_h^{\boldsymbol{\eta}}, \boldsymbol{v})_K + \langle \tau \boldsymbol{u}_h^{\boldsymbol{\eta}} \times \boldsymbol{n}, \boldsymbol{v} \times \boldsymbol{n} \rangle_{\partial K} = \langle \tau \boldsymbol{\eta}, \boldsymbol{v} \times \boldsymbol{n} \rangle_{\partial K},
\end{aligned} \tag{41}$$

for all $(\boldsymbol{r}, \boldsymbol{v}) \in \mathcal{P}_k(K) \times \mathcal{P}_k(K)$. The second local solver maps $\boldsymbol{j}$ to $\left(\boldsymbol{w}_h^{\boldsymbol{j}}, \boldsymbol{u}_h^{\boldsymbol{j}}\right) \in \boldsymbol{P}_k(K) \times \mathcal{P}_k(K)$ such that

$$\begin{aligned}&\left(\mu \boldsymbol{w}_h^{\boldsymbol{j}}, \boldsymbol{r}\right)_K - \left(\boldsymbol{u}_h^{\boldsymbol{j}}, \nabla \times \boldsymbol{r}\right)_K = 0,\\ &\left(\nabla \times \boldsymbol{w}_h^{\boldsymbol{j}} - \epsilon\omega^2 \boldsymbol{u}_h^{\boldsymbol{j}}, \boldsymbol{v}\right)_K + \left\langle \tau \boldsymbol{u}_h^{\boldsymbol{j}} \times \boldsymbol{n}, \boldsymbol{v} \times \boldsymbol{n}\right\rangle_{\partial K} = (\boldsymbol{j}, \boldsymbol{v})_K,\end{aligned} \tag{42}$$

for all $(\boldsymbol{r}, \boldsymbol{v}) \in \boldsymbol{P}_k(K) \times P_k(K)$.

We obtain the following result whose proof can be obtained in the same route as shown in Proposition 3.

Proposition 4. *Let $(\boldsymbol{w}_h, \boldsymbol{u}_h, \hat{\boldsymbol{u}}_h^t)$ be the solution of the HDG method (34). We have that*

$$\begin{aligned}&\boldsymbol{w}_h = \boldsymbol{w}_h^{\boldsymbol{j}} + \boldsymbol{w}_h^{\boldsymbol{\gamma}},\\ &\boldsymbol{u}_h = \boldsymbol{u}_h^{\boldsymbol{j}} + \boldsymbol{u}_h^{\boldsymbol{\gamma}},\\ &\hat{\boldsymbol{u}}_h^t = \boldsymbol{\gamma},\end{aligned} \tag{43}$$

where $\boldsymbol{\gamma} \in \boldsymbol{M}_h^t(\boldsymbol{g})$ satisfies

$$g_h(\boldsymbol{\gamma}, \boldsymbol{\eta}) = r_h(\boldsymbol{\eta}), \quad \forall \boldsymbol{\eta} \in \boldsymbol{M}_h^t(\boldsymbol{0}). \tag{44}$$

Here the forms are given by

$$\begin{aligned}&g_h(\boldsymbol{\xi}, \boldsymbol{\eta}) = \left(\mu \boldsymbol{w}_h^{\boldsymbol{\xi}}, \boldsymbol{w}_h^{\boldsymbol{\eta}}\right)_{\mathcal{T}_h} - \left(\epsilon\omega^2 \boldsymbol{u}_h^{\boldsymbol{\xi}}, \boldsymbol{u}_h^{\boldsymbol{\eta}}\right)_{\mathcal{T}_h} + \left\langle \tau\left(\left(\boldsymbol{u}_h^t\right)^{\boldsymbol{\xi}} - \boldsymbol{\xi}\right), \left(\left(\boldsymbol{u}_h^t\right)^{\boldsymbol{\eta}} - \boldsymbol{\eta}\right)\right\rangle_{\partial \mathcal{T}_h},\\ &r_h(\boldsymbol{\eta}) = \left(\boldsymbol{j}, \boldsymbol{u}_h^{\boldsymbol{\eta}}\right)_{\mathcal{T}_h},\end{aligned} \tag{45}$$

for all $\boldsymbol{\xi}, \boldsymbol{\eta} \in \boldsymbol{M}_h^t$.

We see that the weak formulation (44) involves $\hat{\boldsymbol{u}}_h^t$ only. This is the main advantage of the HDG method for the vector wave equation because it does not need an approximation of the Lagrange multiplier. Therefore, this HDG method is more efficient than the HDG method for the mixed curl–curl formulation. However, it does not enforce the divergence-free condition explicitly.

5. The two-dimensional Maxwell's equations

In this section, we present a detailed implementation of the HDG methods for the time-harmonic Maxwells' equations in two space dimensions. We focus primarily on the HDG method for the mixed curl–curl formulation and describe briefly the HDG method for the vector wave equation at the end of this section.

5.1. Governing equations

In two space dimensions, the mixed curl–curl formulation of the Maxwell's equations in a bounded domain $\Omega \in \mathbb{R}^2$ reads as

$$\begin{aligned}&\mu w - \nabla \times \boldsymbol{u} = 0, \quad \text{in } \Omega,\\ &\nabla \times w - \epsilon\omega^2 \boldsymbol{u} + \epsilon \nabla p = \boldsymbol{j}, \quad \text{in } \Omega,\\ &\nabla \cdot \epsilon \boldsymbol{u} = 0, \quad \text{in } \Omega,\\ &\boldsymbol{u} \times \boldsymbol{n} = g, \quad \text{on} \partial\, \Omega,\\ &p = 0, \quad \text{on } \partial\Omega.\end{aligned} \tag{46}$$

Here $\boldsymbol{u} = (u_x, u_y)$ is the electric field and $w = \mu^{-1}\nabla \times \boldsymbol{u}$ is a scalar variable. We further note that

$$\nabla \times \boldsymbol{u} = \frac{\partial u_y}{\partial x} - \frac{\partial u_x}{\partial y}, \quad \boldsymbol{u} \times \boldsymbol{n} = u_x n_y - u_y n_x, \quad \nabla \times w = \left(\frac{\partial w}{\partial y}, -\frac{\partial w}{\partial x}\right).$$

Note that the cross product of two vectors yield a scalar and the curl of a scalar produces a vector.

Furthermore, the normal component $\boldsymbol{u}^n$ and the tangential component $\boldsymbol{u}^t$ of the vector-valued function $\boldsymbol{u}$ are given by

$$\boldsymbol{u}^n = \left(n_x u^n, n_y u^n\right), \quad \boldsymbol{u}^t = \left(-n_y u^t, n_x u^t\right),$$

where $u^n = \boldsymbol{u} \cdot \boldsymbol{n}$ and $u^t = \boldsymbol{u} \times \boldsymbol{n}$ denote the magnitude of $\boldsymbol{u}^n$ and $\boldsymbol{u}^t$, respectively. We recall our notation that the unit normal vector $\boldsymbol{n} = (n_x, n_y)$ points outward. Therefore, both u^n and u^t change sign across inter-element boundaries since the normal vector $\boldsymbol{n}$ reverses its direction across inter-element boundaries. In particular, we have

$$\begin{aligned}&u^n|_{F^+ \subset \partial K^+} + u^n|_{F^- \subset \partial K^-} = (\boldsymbol{u} \cdot \boldsymbol{n}^+)|_F + (\boldsymbol{u} \cdot \boldsymbol{n}^-)|_F = 0,\\ &u^t|_{F^+ \subset \partial K^+} + u^t|_{F^- \subset \partial K^-} = (\boldsymbol{u} \times \boldsymbol{n}^+)|_F + (\boldsymbol{u} \times \boldsymbol{n}^-)|_F = 0,\end{aligned}$$

where K^+ and K^- are two neighboring elements that share the same edge F, and $F^+ = \lim_{\varepsilon \to 0}(F - \varepsilon \boldsymbol{n}^+)$ and $F^- = \lim_{\varepsilon \to 0}(F - \varepsilon \boldsymbol{n}^-)$ belong to ∂K^+ and $\partial\, K^-$, respectively.

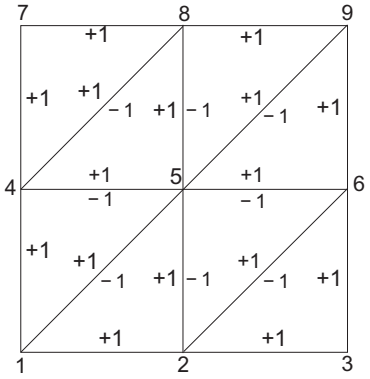

Fig. 1. An illustration of the sign function $\delta_{\partial\mathcal{T}_h}(\boldsymbol{x})$. Note that $\delta_{\partial\mathcal{T}_h}(\boldsymbol{x})$ is equal to 1 on the boundary edges. On the interior edges, $\delta_{\partial\mathcal{T}_h}(\boldsymbol{x})$ is equal 1 on one side and equal to -1 on the other side. For example, $\delta_{\partial\mathcal{T}_h}(\boldsymbol{x})$ is equal to 1 on F_{15} (an edge of the element (1, 5, 4)) and equal to -1 on F_{51} (an edge of the element (1, 2, 5)). This is because the condition $i_a^K < i_b^K$ is satisfied on the edge F_{15}, but not on the edge F_{51}.

5.2. Formulation

To describe the HDG method for numerically solving (46) we introduce a *sign function* $\delta_{\partial\mathcal{T}_h}(\boldsymbol{x})$ which is defined on $\partial\mathcal{T}_h$. (Here we recall that $\partial\mathcal{T}_h = \{\partial K : \forall K \in \mathcal{T}_h\}$ is a collection of boundaries of all elements and that $\mathcal{E}_h^\partial$ is a set of all boundary edges.) Let us consider an element K whose vertices are numbered by global indices $\left(i_1^K, i_2^K, i_3^K\right)$ and whose edges are denoted by $\left(F_{i_1^K i_2^K}, F_{i_2^K i_3^K}, F_{i_3^K i_1^K}\right)$. Here the vertices are listed such that $i_1^K \to i_2^K \to i_3^K \to i_1^K$ follows the counterclockwise direction. Then we define $\delta_{\partial\mathcal{T}_h}(\boldsymbol{x})$ as follows:

$$\delta_{\partial\mathcal{T}_h}\big|_{F_{i_a^K i_b^K}} = \begin{cases} 1 & \text{if } F_{i_a^K i_b^K} \in \mathcal{E}_h^\partial \text{ or } i_a^K < i_b^K \\ -1 & \text{otherwise} \end{cases}, \tag{47}$$

for all $F_{i_a^K i_b^K} \in \left\{F_{i_1^K i_2^K}, F_{i_2^K i_3^K}, F_{i_3^K i_1^K}\right\}$ and for all $K \in \mathcal{T}_h$. Note that $\delta_{\partial\mathcal{T}_h}(\boldsymbol{x})$ is equal to 1 on the boundary edges. On the interior edges, $\delta_{\partial\mathcal{T}_h}(\boldsymbol{x})$ is equal to 1 on the side that satisfies $i_a^K < i_b^K$ and equal to -1 on the other side. An illustration of $\delta_{\partial\mathcal{T}_h}(\boldsymbol{x})$ is shown in Fig. 1.

The HDG method seeks an approximation $(w_h, \boldsymbol{u}_h, p_h, \hat{u}_h^t, \hat{p}_h) \in P_h \times \boldsymbol{V}_h \times P_h \times M_h(g) \times M_h(0)$ such that

$$\begin{aligned}
&(\mu w_h, r)_{\mathcal{T}_h} - (\boldsymbol{u}_h, \nabla \times r)_{\mathcal{T}_h} - \left\langle \delta_{\partial\mathcal{T}_h}\hat{u}_h^t, r\right\rangle_{\partial\mathcal{T}_h} = 0,\\
&(w_h, \nabla \times \boldsymbol{v})_{\mathcal{T}_h} + \langle \hat{w}_h, \boldsymbol{v} \times \boldsymbol{n}\rangle_{\partial\mathcal{T}_h} - (\epsilon\omega^2 \boldsymbol{u}_h, \boldsymbol{v})_{\mathcal{T}_h}\\
&- (p_h, \nabla \cdot \epsilon\boldsymbol{v})_{\mathcal{T}_h} + \langle \epsilon\hat{p}_h, \boldsymbol{v} \cdot \boldsymbol{n}\rangle_{\partial\mathcal{T}_h} = (\boldsymbol{j}, \boldsymbol{v})_{\mathcal{T}_h},\\
&- (\epsilon\boldsymbol{u}_h, \nabla q)_{\mathcal{T}_h} + \left\langle \hat{\boldsymbol{u}}_h^n \cdot \boldsymbol{n}, \epsilon q\right\rangle_{\partial\mathcal{T}_h} = 0,\\
&\langle \hat{w}_h, \delta_{\partial\mathcal{T}_h}\eta\rangle_{\partial\mathcal{T}_h} = 0,\\
&\left\langle \hat{\boldsymbol{u}}_h^n \cdot \boldsymbol{n}, \epsilon\zeta\right\rangle_{\partial\mathcal{T}_h} = 0,
\end{aligned} \tag{48}$$

for all $(r, \boldsymbol{v}, q, \eta, \zeta) \in P_h \times \boldsymbol{V}_h \times P_h \times M_h(0) \times M_h(0)$, where

$$\begin{aligned}
\hat{w}_h &= w_h + \tau_t\left(\boldsymbol{u}_h \times \boldsymbol{n} - \delta_{\partial\mathcal{T}_h}\hat{u}_h^t\right),\\
\hat{\boldsymbol{u}}_h^n &= \boldsymbol{u}_h^n + \tau_n(p_h - \hat{p}_h)\boldsymbol{n}.
\end{aligned} \tag{49}$$

The sign function $\delta_{\partial\mathcal{T}_h}$ is needed because $\hat{u}_h^t \in M_h(g)$ is single-valued on the interior edges and $u^t = \boldsymbol{u} \times \boldsymbol{n}$ changes sign across the interior edges. In particular, $\delta_{\partial\mathcal{T}_h}\hat{u}_h^t$ is nothing but an approximation to u^t on $\partial\mathcal{T}_h$.

5.3. Implementation

The first three equations of (48) defines a local solver that maps $(\hat{u}_h^t, \hat{p}_h, \boldsymbol{j})$ to $(w_h, \boldsymbol{u}_h, p_h)$ as

$$\left(\hat{u}_h^t, \hat{p}_h, \boldsymbol{j}\right) \overset{\mathcal{L}_{2D}}{\mapsto} (w_h, \boldsymbol{u}_h, p_h), \tag{50}$$

where $(w_h, \boldsymbol{u}_h, p_h) \in \mathcal{P}_k(K) \times \boldsymbol{\mathcal{P}}_k(K) \times P_k(K)$ satisfies

$$
\begin{aligned}
&(\mu w_h, r)_K - (\boldsymbol{u}_h, \nabla \times r)_K = \langle \delta_{\partial\mathcal{T}_h} \hat{u}_h^t, r\rangle_{\partial K},\\
&(\nabla \times w_h, \boldsymbol{v})_K + \langle \tau_t \boldsymbol{u}_h \times \boldsymbol{n}, \boldsymbol{v} \times \boldsymbol{n}\rangle_{\partial K} - (p_h, \nabla \cdot \epsilon \boldsymbol{v})_K - (\epsilon\omega^2 \boldsymbol{u}_h, \boldsymbol{v})_K = (\boldsymbol{j}, \boldsymbol{v})_K - \langle \epsilon \hat{p}_h, \boldsymbol{v} \cdot \boldsymbol{n}\rangle_{\partial K} + \left\langle \tau_t \delta_{\partial\mathcal{T}_h} \hat{u}_h^t, \boldsymbol{v} \times \boldsymbol{n}\right\rangle_{\partial K},\\
&(\nabla \cdot \epsilon \boldsymbol{u}_h, q)_K + \langle \tau_n p_h, \epsilon q\rangle_{\partial K} = \langle \tau_n \hat{p}_h, \epsilon q\rangle_{\partial K},
\end{aligned}
\tag{51}
$$

for all $(r, \boldsymbol{v}, q) \in \mathcal{P}_k(K) \times \boldsymbol{\mathcal{P}}_k(K) \times P_k(K)$ and for all $K \in \mathcal{T}_h$. For any pair $(\xi, \varrho) \in M_h \times M_h$ we introduce

$$
\begin{aligned}
&\left(w_h^{\xi}, \boldsymbol{u}_h^{\xi}, p_h^{\xi}\right) := \mathcal{L}_{2D}(\xi, 0, 0),\\
&\left(w_h^{\varrho}, \boldsymbol{u}_h^{\varrho}, p_h^{\varrho}\right) := \mathcal{L}_{2D}(0, \varrho, 0),\\
&\left(w_h^{\boldsymbol{j}}, \boldsymbol{u}_h^{\boldsymbol{j}}, p_h^{\boldsymbol{j}}\right) := \mathcal{L}_{2D}(0, 0, \boldsymbol{j}),
\end{aligned}
\tag{52}
$$

where $\left(w_h^{\xi}, \boldsymbol{u}_h^{\xi}, p_h^{\xi}\right)$, $\left(w_h^{\varrho}, \boldsymbol{u}_h^{\varrho}, p_h^{\varrho}\right)$, and $\left(w_h^{\boldsymbol{j}}, \boldsymbol{u}_h^{\boldsymbol{j}}, p_h^{\boldsymbol{j}}\right)$ are obtained from (51) when we replace $(\hat{u}_h^t, \hat{p}_h, \boldsymbol{j})$ with $(\xi, 0, 0)$, $(0, \varrho, 0)$, and $(0, 0, \boldsymbol{j})$, respectively.

It then follows that

$$
\begin{aligned}
&w_h = w_h^{\lambda} + w_h^{\rho} + w_h^{\boldsymbol{j}},\\
&\boldsymbol{u}_h = \boldsymbol{u}_h^{\lambda} + \boldsymbol{u}_h^{\rho} + \boldsymbol{u}_h^{\boldsymbol{j}},\\
&p_h = p_h^{\lambda} + p_h^{\rho} + p_h^{\boldsymbol{j}},\\
&\hat{u}_h^t = \lambda,\\
&\hat{p}_h = \rho,
\end{aligned}
\tag{53}
$$

where $(\lambda, \rho) \in M_h(0) \times M_h(0)$ satisfies

$$
\begin{aligned}
&a_h(\lambda, \eta) + b_h(\rho, \eta) = \ell_h(\eta), \quad \forall \eta \in M_h(0),\\
&-b_h(\zeta, \lambda) + c_h(\rho, \zeta) = f_h(\zeta), \quad \forall \zeta \in M_h(0).
\end{aligned}
\tag{54}
$$

Here the forms are given by

$$
\begin{aligned}
&a_h(\xi, \eta) = \left(\mu w_h^{\eta}, w_h^{\xi}\right)_{\mathcal{T}_h} - \left(\epsilon\omega^2 \boldsymbol{u}_h^{\eta}, \boldsymbol{u}_h^{\xi}\right)_{\mathcal{T}_h} + \left\langle \tau_n \epsilon p_h^{\eta}, p_h^{\xi}\right\rangle_{\partial\mathcal{T}_h} + \left\langle \tau_t\left(\boldsymbol{u}_h^{\eta} \times \boldsymbol{n} - \delta_{\partial\mathcal{T}_h}\eta\right), \left(\boldsymbol{u}_h^{\xi} \times \boldsymbol{n} - \delta_{\partial\mathcal{T}_h}\xi\right)\right\rangle_{\partial\mathcal{T}_h},\\
&b_h(\varrho, \eta) = \left\langle \tau_n p_h^{\eta}, \epsilon\varrho\right\rangle_{\partial\mathcal{T}_h} + \left\langle \epsilon\varrho, \boldsymbol{u}_h^{\eta} \cdot \boldsymbol{n}\right\rangle_{\partial\mathcal{T}_h},\\
&c_h(\varrho, \zeta) = \left(\mu w_h^{\varrho}, w_h^{\zeta}\right)_{\mathcal{T}_h} - \left(\epsilon\omega^2 \boldsymbol{u}_h^{\varrho}, \boldsymbol{u}_h^{\zeta}\right)_{\mathcal{T}_h} + \left\langle \tau_t \boldsymbol{u}_h^{\varrho} \times \boldsymbol{n}, \boldsymbol{u}_h^{\zeta} \times \boldsymbol{n}\right\rangle_{\partial\mathcal{T}_h} + \left\langle \tau_n \epsilon\left(p_h^{\varrho} - \varrho\right), \left(p_h^{\zeta} - \zeta\right)\right\rangle_{\partial\mathcal{T}_h},\\
&\ell_h(\eta) = \left(\boldsymbol{j}, \boldsymbol{u}_h^{\eta}\right)_{\mathcal{T}_h},\\
&f_h(\zeta) = -\left(\boldsymbol{j}, \boldsymbol{u}_h^{\zeta}\right)_{\mathcal{T}_h},
\end{aligned}
\tag{55}
$$

for all $\xi, \eta \in M_h$ and $\varrho, \zeta \in M_h$.

The weak formulation (54) gives rise to a system of equations of the form

$$
\begin{pmatrix} A & B\\ -B^T & C \end{pmatrix} \begin{pmatrix} \Lambda\\ \Phi \end{pmatrix} = \begin{pmatrix} L\\ F \end{pmatrix},
\tag{56}
$$

where Λ and Φ represent the vector of degrees of freedom of λ and ρ, respectively. The matrices and vectors in (56) correspond to the bilinear forms and linear forms in (54) in the order they appear in the equation. In order to form the global matrices A, B, C and vectors F, L, we need to compute their elemental quantities. For example, to form A, we compute its elemental matrices as

$$
A_{ij}^K := a_h(\varphi_i^K, \varphi_j^K) = \left(\mu w_h^{\varphi_i^K}, w_h^{\varphi_j^K}\right)_K - \left(\epsilon\omega^2 \boldsymbol{u}_h^{\varphi_i^K}, \boldsymbol{u}_h^{\varphi_j^K}\right)_K + \left\langle \tau_n \epsilon p_h^{\varphi_i^K}, p_h^{\varphi_j^K}\right\rangle_{\partial K} + \left\langle \tau_t\left(\boldsymbol{u}_h^{\varphi_i^K} \times \boldsymbol{n} - \delta_{\partial\mathcal{T}_h}\varphi_i^K\right), \left(\boldsymbol{u}_h^{\varphi_j^K} \times \boldsymbol{n} - \delta_{\partial\mathcal{T}_h}\varphi_j^K\right)\right\rangle_{\partial K},
$$

for all $K \in \mathcal{T}_h$, where φ_i^K are polynomials of degree k defined over three edges of the element boundary ∂K. Note that since there are $k+1$ polynomials on each edge, there are $3(k+1)$ polynomials per element. Hence, the size of A^K is $3(k+1) \times 3(k+1)$. We thus need to compute $\left(w_h^{\varphi_i^K}, \boldsymbol{u}_h^{\varphi_i^K}, p_h^{\varphi_i^K}\right)$ by using $\eta = \varphi_i^K$ in (52). Once the elemental matrices are computed for all elements the global matrix A can be assembled by using the standard finite element assembly. The other global matrices and vectors can be formed in the same way.

5.4. Computational complexity and storage requirement

We discuss here the computational complexity and memory storage required by the HDG method. First, we need to solve the local solver (52) for all elements. On each element the local problem requires us to invert the matrix of size $M \times M$, where $M = 2(k+1)(k+2)$ is the degrees of freedom $(w_h, \boldsymbol{u}_h, p_h)$ on each element. The computational cost of the local part is thus $O(N_K M^3)$, where N^K is the number of elements.

Next, we point out the degrees of freedom and sparsity structure of the linear system (56), restricting our attention to the case of a conforming triangulation $\mathcal{T}_h$ (no hanging nodes). It is clear that the matrix A has a block structure with square blocks of size $(k+1)\times(k+1)$ for each edge F. The number of block rows and block columns is equal to N_F, where $N_F \approx 3N_K/2$ is the number of interior edges of the triangulation. Hence, the size of the matrix A is $N_A \times N_A$, where $N_A = (k+1)\,N_F$. Furthermore, on each block row, there are at most 5 nonzero blocks. Hence, the number of nonzero entries of A is $5(k+1)^2 N_F$. The other matrices B and C have the same size and number of nonzero entries as A. The solution of the linear system (56) will typically cost $O((2N_A)^\gamma)$ with $\gamma \approx 2$. Therefore, the computational complexity of the HDG method will be dominated by the cost of solving the system (56) since the operation count of the local solvers scales linearly with N_K.

5.5. The HDG method for the vector wave equation

Finally, we close this section by briefly describing the HDG method for the two-dimensional vector wave equation

$$\begin{aligned} &\mu w - \nabla\times \boldsymbol{u} = 0, \quad \text{in } \Omega,\\ &\nabla\times w - \epsilon\omega^2 \boldsymbol{u} = \boldsymbol{j}, \quad \text{in } \Omega,\\ &\boldsymbol{u}\times\boldsymbol{n} = 0, \quad \text{on } \partial\Omega. \end{aligned} \tag{57}$$

The HDG method for this system finds an approximation $(w_h, \boldsymbol{u}_h, \hat{u}_h^t) \in P_h \times \boldsymbol{V}_h \times M_h(g)$ such that

$$\begin{aligned} &(\mu w_h, r)_{\mathcal{T}_h} - (\boldsymbol{u}_h, \nabla\times r)_{\mathcal{T}_h} - \langle \delta_{\partial\mathcal{T}_h}\hat{u}_h^t, r\rangle_{\partial\mathcal{T}_h} = 0,\\ &(w_h, \nabla\times\boldsymbol{v})_{\mathcal{T}_h} + \langle \hat{w}_h, \boldsymbol{v}\times\boldsymbol{n}\rangle_{\partial\mathcal{T}_h} - (\epsilon\omega^2\boldsymbol{u}_h, \boldsymbol{v})_{\mathcal{T}_h} = (\boldsymbol{j}, \boldsymbol{v})_{\mathcal{T}_h},\\ &\langle \hat{w}_h, \delta_{\partial\mathcal{T}_h}\eta\rangle_{\partial\mathcal{T}_h} = 0, \end{aligned} \tag{58}$$

for all $(r, \boldsymbol{v}, \eta) \in P_h \times \boldsymbol{V}_h \times M_h(0)$, where

$$\hat{w}_h = w_h + \tau_t(\boldsymbol{u}_h\times\boldsymbol{n} - \delta_{\partial\mathcal{T}_h}\hat{u}_h^t). \tag{59}$$

The method is implemented by using the hybridization technique as described below.

For any given $\xi \in M_h$ we define $(w_h^\xi, \boldsymbol{u}_h^\xi) \in \mathcal{P}_k(K)\times\boldsymbol{\mathcal{P}}_k(K)$ such that

$$\begin{aligned} &(\mu w_h^\xi, r)_K - (\boldsymbol{u}_h^\xi, \nabla\times r)_K = \langle \delta_{\partial\mathcal{T}_h}\xi, r\rangle_{\partial K},\\ &(\nabla\times w_h^\xi, \boldsymbol{v})_K - (\epsilon\omega^2\boldsymbol{u}_h^\xi, \boldsymbol{v})_K + \langle \tau_t\boldsymbol{u}_h^\xi\times\boldsymbol{n}, \boldsymbol{v}\times\boldsymbol{n}\rangle_{\partial K} = \langle \tau_t\delta_{\partial\mathcal{T}_h}\xi, \boldsymbol{v}\times\boldsymbol{n}\rangle_{\partial K}, \end{aligned} \tag{60}$$

and $\left(w_h^{\boldsymbol{j}}, \boldsymbol{u}_h^{\boldsymbol{j}}\right) \in \mathcal{P}_k(K)\times\boldsymbol{\mathcal{P}}_k(K)$ such that

$$\begin{aligned} &\left(\mu w_h^{\boldsymbol{j}}, r\right)_K - \left(\boldsymbol{u}_h^{\boldsymbol{j}}, \nabla\times r\right)_K = 0,\\ &\left(\nabla\times w_h^{\boldsymbol{j}}, \boldsymbol{v}\right)_K - \left(\epsilon\omega^2\boldsymbol{u}_h^{\boldsymbol{j}}, \boldsymbol{v}\right)_K + \left\langle \tau_t\boldsymbol{u}_h^{\boldsymbol{j}}\times\boldsymbol{n}, \boldsymbol{v}\times\boldsymbol{n}\right\rangle_{\partial K} = (\boldsymbol{j}, \boldsymbol{v})_K, \end{aligned} \tag{61}$$

for all $(r, \boldsymbol{v}) \in \mathcal{P}_k(K)\times\boldsymbol{\mathcal{P}}_k(K)$ and for all $K \in \mathcal{T}_h$.

It then follows that the HDG solution is computed as

$$\begin{aligned} &w_h = w_h^\phi + w_h^{\boldsymbol{j}},\\ &\boldsymbol{u}_h = \boldsymbol{u}_h^\phi + \boldsymbol{u}_h^{\boldsymbol{j}},\\ &\hat{u}_h^t = \phi, \end{aligned} \tag{62}$$

where $\phi \in M_h(g)$ satisfies

$$s_h(\phi, \eta) = r_h(\eta), \quad \forall \eta \in M_h(0), \tag{63}$$

Here the forms are given by

$$\begin{aligned} &s_h(\xi, \eta) = (\mu w_h^\eta, w_h^\xi)_{\mathcal{T}_h} - (\epsilon\omega^2\boldsymbol{u}_h^\eta, \boldsymbol{u}_h^\xi)_{\mathcal{T}_h} + \langle \tau_t(\boldsymbol{u}_h^\eta\times\boldsymbol{n} - \delta_{\partial\mathcal{T}_h}\eta), (\boldsymbol{u}_h^\xi\times\boldsymbol{n} - \delta_{\partial\mathcal{T}_h}\xi)\rangle_{\partial\mathcal{T}_h},\\ &r_h(\eta) = (\boldsymbol{j}, \boldsymbol{u}_h^\eta)_{\mathcal{T}_h}, \end{aligned} \tag{64}$$

for all $\xi, \eta \in M_h$.

The above weak formulation results in a linear system of the form

$$G\Phi = R, \tag{65}$$

where Φ represents the vector of degrees of freedom of ϕ. The matrix G and vector R can be formed by computing the elemental matrices and vectors in the same way as . It is clear that the HDG method for the vector wave equation requires only 1/3 memory storage of the method for the mixed curl–curl formulation. Moreover, the cost of solving the linear system (65) can be significantly less than that of solving the system (56) because the dimension of the linear system (65) is only half of that of the system (56). This HDG method is more efficient than the method for the mixed curl–curl formulation.

6. Local postprocessing

In this section we propose a new local postprocessing to obtain a $\boldsymbol{H}^{\mathrm{curl}}$-conforming approximation $\boldsymbol{u}_h^*$ which converges with an additional order in the $\boldsymbol{H}^{\mathrm{curl}}$-norm. We consider here the two-dimensional case with triangular elements.

6.1. Postprocessing scheme

We find $\boldsymbol{u}_h^*$ as the element of $\boldsymbol{\mathcal{P}}_{k+1}(K)$ such that for all $K \in \mathcal{T}_h$,

$$\begin{aligned} &\langle \boldsymbol{u}_h^* \times \boldsymbol{n} - \delta_{\partial \mathcal{T}_h} \hat{u}_h^t, \eta \rangle_F = 0, \quad \forall \eta \in \mathcal{P}_{k+1}(F), \forall F \in \partial K, \\ &\left(\boldsymbol{u}_h^* - \boldsymbol{u}_h, \nabla \times w\right)_K = 0, \quad \forall w \in \mathcal{P}_k(K), \\ &\left(\nabla \cdot (\boldsymbol{u}_h^* - \boldsymbol{u}_h), s\right)_K = 0, \quad \forall s \in \mathcal{P}_{k-1}(K). \end{aligned} \tag{66}$$

This new approximation $\boldsymbol{u}_h^*$ is well-defined and $\boldsymbol{H}^{\mathrm{curl}}(\Omega)$-conforming, as we show next. Note that to compute $\boldsymbol{u}_h^*$ we need only to invert a matrix of size equal to the dimension of $\boldsymbol{\mathcal{P}}_{k+1}(K)$ for each element K of the triangulation $\mathcal{T}_h$. Hence, the new approximation is less expensive to compute than the original approximation. Moreover, numerical results presented in the next section show that $\boldsymbol{u}_h^*$ converges with order $k+1$ in the $\boldsymbol{H}^{\mathrm{curl}}(\mathcal{T}_h)$-norm, whereas $\boldsymbol{u}_h$ converges with order k in the $\boldsymbol{H}^{\mathrm{curl}}(\Omega)$-norm.

6.2. Well-posedness of the postprocessing scheme

We now prove that the local postprocessing scheme is well-posed.

Proposition 5. *Suppose that all the triangles $K \in \mathcal{T}_h$ are acute. Then the postprocessed solution $\boldsymbol{u}_h^*$ given in (66) is well-defined and conforming in the space $H^{\mathrm{curl}}(\Omega)$.*

Proof. Let us show that $\boldsymbol{u}_h^*$ given in (66) is well-defined. We verify first the equality between the number of degrees of freedom and the dimension of $\boldsymbol{\mathcal{P}}_{k+1}(K)$:

$$\dim(\boldsymbol{\mathcal{P}}_{k+1}(K)) = (k+2)(k+3). \tag{67}$$

The number of degrees of freedom in the first equation of (66) is three times the dimension of $\mathcal{P}_{k+1}(\vec{F})$:

$$3(k+2). \tag{68}$$

The number of degrees of freedom in the second equation of (66) is the dimension of $\mathcal{P}_k(K)$ minus one:

$$\frac{(k+1)(k+2)}{2} - 1. \tag{69}$$

The number of degrees of freedom in the third equation of (66) is the dimension of $\mathcal{P}_{k-1}(K)$:

$$\frac{k(k+1)}{2}. \tag{70}$$

The total number of degrees of freedom is exactly equal to $\dim(\boldsymbol{\mathcal{P}}_{k+1}(K))$.

This means that to prove the existence and uniqueness of $\boldsymbol{u}_h^*$, we only need to show that $\boldsymbol{u}_h^* = \boldsymbol{0}$ is the unique solution of (66) when $\hat{u}_h^t = 0$ and $u_h = \boldsymbol{0}$. To do that, we begin by noting that the first equation of (66) implies that

$$\boldsymbol{u}_h^* \times \boldsymbol{n} = 0, \quad \text{on each edge}. \tag{71}$$

Integrating the second equation of (66) by parts and using (71) we obtain

$$\left(\nabla \times \boldsymbol{u}_h^*, w\right)_K = 0, \quad \forall w \in \mathcal{P}_k(K), \tag{72}$$

which yields

$$\boldsymbol{u}_h^* = \nabla \psi, \quad \psi \in \mathcal{P}_{k+2}(K). \tag{73}$$

Eqs. (71) and (73) show that ψ is constant along ∂K. Since this constant can be chosen arbitrarily, we take it to be zero. Thus, we can write that $\psi = \lambda_1 \lambda_2 \lambda_3 \eta$ where λ_i is the so-called ith barycentric coordinate function associated to the triangle K and η is an element of $\mathcal{P}_{k-1}(K)$.

Substituting (73) into the third equation of (66), and setting b colone $\lambda_1 \lambda_2 \lambda_3$, we obtain, for all $s \in \mathcal{P}_{k-1}(K)$,

$$0 = (\nabla^2(b\eta), s)_K = -(\nabla(b\eta), \nabla s)_K + \langle \boldsymbol{n} \cdot \nabla(b\eta), s \rangle_{\partial K}.$$

Taking $s := \eta$, we get

$$\begin{aligned} 0 &= -(\nabla(b\eta), \nabla\eta)_K + \langle \boldsymbol{n} \cdot \nabla b, \eta^2 \rangle_{\partial K} = -(b\nabla\eta, \nabla\eta)_K - \frac{1}{2}(\nabla b, \nabla\eta^2)_K + \langle \boldsymbol{n} \cdot \nabla b, \eta^2 \rangle_{\partial K} \\ &= -(b\nabla\eta, \nabla\eta)_K + \frac{1}{2}(\nabla^2 b, \eta^2)_K + \frac{1}{2}\langle \boldsymbol{n} \cdot \nabla b, \eta^2 \rangle_{\partial K}. \end{aligned}$$

We claim that the intregrands in the three terms are nonnegative. As a consequence, we get that $\eta = 0$. Hence, we have $\boldsymbol{u}_h^* = \nabla\psi = 0$.

It remains to prove the claim. But, we clearly have that $b \geqslant 0$ in K. Moreover, on the face of the triangle K such that $\lambda_1 = 0$, we have that

$$\boldsymbol{n}\cdot\nabla b = (\boldsymbol{n}_1\cdot\nabla\lambda_1)\lambda_2\lambda_3 \leqslant 0,$$

since $\nabla\lambda_1 = -|e_1|n_1/(2|K|)$. A similar argument shows that $n\cdot\nabla b \leqslant 0$ on the two remaining faces. Note that we have still not used the fact that the triangle K is acute. We are going to use this to show that $\nabla^2 b \leqslant 0$. Indeed, a simple computation gives us that

$$\nabla^2 b = \frac{1}{2|K|^2}\left(|e_1||e_2|\boldsymbol{n_1}\cdot\boldsymbol{n}_2\lambda_3 + |e_2||e_3|\boldsymbol{n_2}\cdot\boldsymbol{n}_3\lambda_1 + |e_3||e_1|\boldsymbol{n_3}\cdot\boldsymbol{n}_1\lambda_2\right) \leqslant 0,$$

when the triangle K is acute. This proves the claim.

Finally, it follows from the first equation of (66) that

$$\boldsymbol{u}_h^{*t} := \boldsymbol{n}\times\boldsymbol{u}_h^*\times\boldsymbol{n} = \boldsymbol{n}\times\delta_{\partial\mathcal{T}_h}\hat{u}_h^t. \tag{74}$$

Hence, $\boldsymbol{u}_h^{*t}$ is *continuous* across the element boundaries since $\hat{u}_h^t \in M_h$. This implies that $\boldsymbol{u}_h^*$ resides in the space $H^{\mathrm{curl}}(\Omega)$. This completes the proof. □

The **Curl** of the postprocessed approximation satisfies and interesting relation, as we see in the following result.

Lemma 6.1. *The postprocessed solution $\boldsymbol{u}_h^*$ given in (66) satisfies*

$$\left(\nabla\times\boldsymbol{u}_h^*, q\right)_K = (\mu w_h, q)_K, \quad \forall q\in\mathcal{P}_k(K). \tag{75}$$

Proof. We note from the first equation of (48) that

$$(\boldsymbol{u}_h, \nabla\times q)_K = (\mu w_h, q)_K - \left\langle\delta_{\partial\mathcal{T}_h}\hat{u}_h^t, q\right\rangle_{\partial K}, \quad \forall q\in\mathcal{P}_k(K). \tag{76}$$

It thus follows from the first two equations of (66) that

$$\left(\boldsymbol{u}_h^*, \nabla\times q\right)_K = (\mu w_h, q)_K - \left\langle\boldsymbol{u}_h^*\times\boldsymbol{n}, q\right\rangle_{\partial K}, \quad \forall q\in\mathcal{P}_k(K), \tag{77}$$

which, after integration by parts, yields the desired result. This completes the proof. □

This lemma shows that $\nabla\times\boldsymbol{u}_h^*$ has the same accuracy and convergence rate as w_h.

7. Numerical experiments

In this section, we present numerical experiments to assess the performance and accuracy of the two HDG methods. We consider two-dimensional model problems that have been studied in [1,23]. In all of these examples, we select the stabilization parameters according to (9) and (36). In order to study the convergence and accuracy of the methods we define the error in the L^2-norm as

$$\|\boldsymbol{u}-\boldsymbol{u}_h\|_{\mathcal{T}_h} = \left(\sum_{K\in\mathcal{T}_h}\int_K\|\boldsymbol{u}-\boldsymbol{u}_h\|^2\right)^{1/2}, \tag{78}$$

and the error in the $\boldsymbol{H}^{\mathrm{curl}}(\mathcal{T}_h)$-norm as

$$\|\boldsymbol{u}-\boldsymbol{u}_h\|_{\boldsymbol{H}^c} = \left(\sum_{K\in\mathcal{T}_h}\int_K\left(\|\boldsymbol{u}-\boldsymbol{u}_h\|^2 + \|\nabla\times\boldsymbol{u}-\nabla\times\boldsymbol{u}_h\|^2\right)\right)^{1/2}. \tag{79}$$

We shall refer to the HDG method for the mixed curl–curl formulation as HDG-I and the HDG method for the vector wave equation as HDG-II.

7.1. The square domain problem

In the first example, we consider solving the time-harmonic Maxwell's equations in a square domain $\Omega = (-1,1)\times(-1,1)$ with $\mu = \epsilon = 1$. Furthermore, we set $\boldsymbol{j} = 0$ and select suitable boundary data g so that the problem has the following exact solution

$$\boldsymbol{u} = (\sin(\omega y), \sin(\omega x)).$$

In [23] this example is used to investigate the convergence of the IP method on a sequence of unstructured triangular meshes for different polynomial degrees and frequencies ω. It is shown in [23] that the approximate solution of the IP method converges with order k in the $\boldsymbol{H}^{\mathrm{curl}}(\mathcal{T}_h)$-norm and with order $k+1$ in the L^2-norm.

We demonstrate the convergence and accuracy of the HDG methods on a sequence of unstructured meshes. More specially, we start with an unstructured mesh of 16 elements as shown in Fig. 2(a) and successively refine this initial mesh by subdividing every element into four smaller elements. As shown in Fig. 2(b) the finest mesh consists of 4096 elements and is obtained after we refine the initial mesh four times. On these meshes, we consider polynomials of degree $k = 1, 2, 3$ to represent all the approximate variables.

We present in Tables 1–3 numerical results obtained for $\omega = 1, 2$ and 4, respectively. In each case we show the polynomial degree k, the number of elements in the computational mesh n_e, as well as the error and the order of convergence for both HDG-I and HDG-II. We observe that for both the HDG methods the approximation error converges to zero at the optimal rate $O(h^{k+1})$ in the L^2-norm and at the rate $O(h^k)$ in the $\boldsymbol{H}^{\mathrm{curl}}(\mathcal{T}_h)$-norm. The convergence rate of the approximate vector field of the HDG methods is thus similar to that of the IP method. However, we note that the postprocessed vector field $\boldsymbol{u}_h^*$ converges to the exact solution $\boldsymbol{u}$ at the rate $O(h^{k+1})$ in the $\boldsymbol{H}^{\mathrm{curl}}(\Omega)$-norm, which is one order higher than the convergence rate of the approximate vector field $\boldsymbol{u}_h$. Moreover, $\boldsymbol{u}_h^*$ is $\boldsymbol{H}^{\mathrm{curl}}(\Omega)$-conforming and inexpensive to compute. As a result, both the HDG-I and HDG-II methods outperform the IP method for the same number of elements.

Furthermore, we see that the approximation error increases with the frequency for a given fixed mesh and fixed polynomial degree. We also observe that the approximation error decreases rapidly when either the mesh is refined or the polynomial degree is increased as we would expect for this smooth problem. We would like to point out that HDG-I and HDG-II perform equally well in terms of accuracy and convergence rate. However, HDG-II is more computationally efficient than HDG-I because the former has less globally coupled degrees of freedom than the latter.

Finally, we investigate how the condition number of the global stiffness matrix depends on the polynomial degree k, the number of elements n_e and the frequency ω. To this end we define the condition number ratio R as

$$R = \frac{C}{15(3k^{1.4} - 1)n_e\omega^{-2}},$$

where C is the condition number of the stiffness matrix G (65) of the HDG-II method. Here the condition number is defined as the ratio of the largest singular value of G to the smallest singular value, which are computed by a singular value decomposition of G. We report in Table 4 the condition number ratio R as a function of k, n_e and ω. We see that the condition number ratio R is close to 1. The results show that the condition number grows linearly with the number of elements n_e as both k and ω are fixed. It is interesting to note that for the range of frequency considered here the condition number decreases as the frequency ω increases. More specifically, the condition number is proportional to ω^{-2} as both k and n_e are kept fixed.

7.2. The L-shaped domain problem with smooth solution

We consider the time-harmonic Maxwell's equations in a L-shaped domain $\Omega = (-1, 1)^2 \backslash [0, 1) \times (-1, 0]$ with $\epsilon = \mu = 1$. We set $\boldsymbol{j} = 0$ and select suitable boundary data g so that the problem has an exact solution of the form

$$\boldsymbol{u} = \nabla \times f, \tag{80}$$

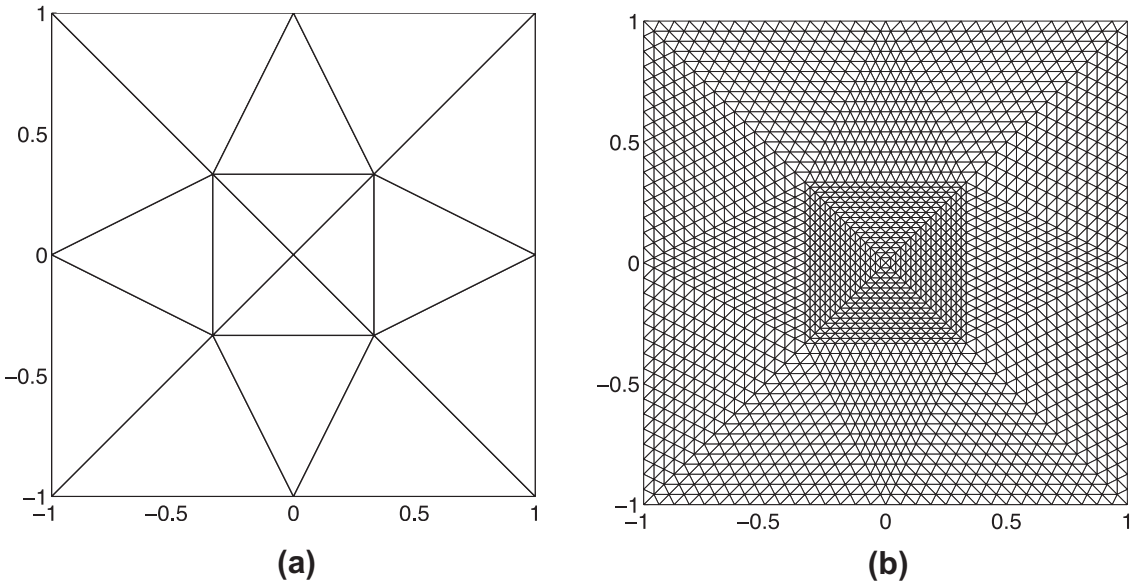

Fig. 2. The initial mesh (a) and the mesh after four refinements (b) for the square domain.

Table 1
Example 1: History of convergence of the HDG methods for $\omega = 1$.

Degree k	Mesh n_e	HDG-I						HDG-II					
		$\|\boldsymbol{u}-\boldsymbol{u}_h\|_{\mathcal{T}_h}$		$\|\boldsymbol{u}-\boldsymbol{u}_h\|_{\boldsymbol{H}^c}$		$\|\boldsymbol{u}-\boldsymbol{u}_h^*\|_{\boldsymbol{H}^c}$		$\|\boldsymbol{u}-\boldsymbol{u}_h\|_{\mathcal{T}_h}$		$\|\boldsymbol{u}-\boldsymbol{u}_h\|_{\boldsymbol{H}^c}$		$\|\boldsymbol{u}-\boldsymbol{u}_h^*\|_{\boldsymbol{H}^c}$	
		Error	Order	Error	Order	Error	Order	Error	Order	Error	Order	Error	Order
1	16	4.20e−2	–	2.26e−1	–	6.48e−2	–	5.49e−2	–	2.68e−1	–	6.17e−2	–
	64	1.09e−2	1.94	1.27e−1	0.83	1.59e−2	2.03	1.27e−2	2.11	1.33e−1	1.01	1.51e−2	2.03
	256	2.80e−3	1.96	6.65e−2	0.93	3.93e−3	2.01	3.09e−3	2.04	6.60e−2	1.01	3.73e−3	2.01
	1024	7.11e−4	1.98	3.39e−2	0.97	9.77e−4	2.01	7.62e−4	2.02	3.29e−2	1.00	9.29e−4	2.01
	4096	1.79e−4	1.99	1.71e−2	0.99	2.44e−4	2.00	1.89e−4	2.01	1.64e−2	1.00	2.32e−4	2.00
2	16	3.26e−3	–	4.56e−2	–	3.60e−3	–	3.25e−3	–	4.27e−2	–	3.30e−3	–
	64	3.99e−4	3.03	1.09e−2	2.06	4.48e−4	3.01	4.35e−4	2.90	1.08e−2	1.99	4.13e−4	3.00
	256	4.92e−5	3.02	2.65e−3	2.04	5.60e−5	3.00	5.54e−5	2.97	2.69e−3	2.00	5.18e−5	3.00
	1024	6.09e−6	3.01	6.54e−4	2.02	7.01e−6	3.00	6.98e−6	2.99	6.72e−4	2.00	6.48e−6	3.00
	4096	7.58e−7	3.01	1.62e−4	2.01	8.78e−7	3.00	8.75e−7	3.00	1.68e−4	2.00	8.11e−7	3.00
3	16	1.61e−4	–	2.43e−3	–	2.03e−4	–	2.24e−4	–	3.51e−3	–	1.90e−4	–
	64	1.04e−5	3.95	3.34e−4	2.86	1.27e−5	4.00	1.30e−5	4.10	4.24e−4	3.05	1.18e−5	4.01
	256	6.66e−7	3.96	4.40e−5	2.93	7.85e−7	4.01	7.88e−7	4.05	5.21e−5	3.02	7.38e−7	4.00
	1024	4.23e−8	3.98	5.64e−6	2.96	4.88e−8	4.01	4.85e−8	4.02	6.46e−6	3.01	4.60e−8	4.00
	4096	2.66e−9	3.99	7.14e−7	2.98	3.04e−9	4.01	3.01e−9	4.01	8.04e−7	3.01	2.87e−9	4.00

Table 2
Example 1: History of convergence of the HDG methods for $\omega = 2$.

Degree k	Mesh n_e	HDG-I						HDG-II					
		$\|\boldsymbol{u}-\boldsymbol{u}_h\|_{\mathcal{T}_h}$		$\|\boldsymbol{u}-\boldsymbol{u}_h\|_{\boldsymbol{H}^c}$		$\|\boldsymbol{u}-\boldsymbol{u}_h^*\|_{\boldsymbol{H}^c}$		$\|\boldsymbol{u}-\boldsymbol{u}_h\|_{\mathcal{T}_h}$		$\|\boldsymbol{u}-\boldsymbol{u}_h\|_{\boldsymbol{H}^c}$		$\|\boldsymbol{u}-\boldsymbol{u}_h^*\|_{\boldsymbol{H}^c}$	
		Error	Order	Error	Order	Error	Order	Error	Order	Error	Order	Error	Order
1	16	1.98e−1	–	1.46e−0	–	4.80e−1	–	2.74e−1	–	1.73e−0	–	3.17e−1	–
	64	4.71e−2	2.07	7.90e−1	0.89	1.05e−1	2.19	5.8e−2	2.24	8.13e−1	1.09	8.03e−2	1.98
	256	1.20e−2	1.98	4.07e−1	0.96	2.56e−2	2.04	1.38e−2	2.07	3.99e−1	1.03	2.01e−2	2.00
	1024	3.02e−3	1.99	2.06e−1	0.98	6.34e−3	2.01	3.39e−3	2.03	1.98e−1	1.01	5.03e−3	2.00
	4096	7.58e−4	1.99	1.03e−1	0.99	1.58e−3	2.00	8.39e−4	2.01	9.87e−2	1.01	1.26e−3	2.00
2	16	2.66e−2	–	3.63e−1	–	5.05e−2	–	2.68e−2	–	3.72e−1	–	4.92e−2	–
	64	3.18e−3	3.06	8.29e−2	2.13	6.17e−3	3.03	3.57e−3	2.91	9.03e−2	2.04	5.79e−3	3.09
	256	3.89e−4	3.03	1.99e−2	2.06	7.72e−4	3.00	4.48e−4	2.99	2.22e−2	2.03	7.18e−4	3.01
	1024	4.80e−5	3.02	4.85e−3	2.03	9.68e−5	3.00	5.61e−5	3.00	5.48e−3	2.02	8.95e−5	3.00
	4096	5.96e−6	3.01	1.20e−3	2.02	1.21e−5	3.00	7.00e−6	3.00	1.36e−3	2.01	1.12e−5	3.00
3	16	2.58e−3	–	4.53e−2	–	5.45e−3	–	3.59e−3	–	5.63e−2	–	4.16e−3	–
	64	1.69e−4	3.93	6.34e−3	2.84	3.54e−4	3.95	2.06e−4	4.13	6.96e−3	3.02	2.83e−4	3.88
	256	1.08e−5	3.97	8.24e−4	2.94	2.22e−5	3.99	1.25e−5	4.04	8.60e−4	3.02	1.79e−5	3.98
	1024	6.87e−7	3.98	1.05e−4	2.97	1.39e−6	4.00	7.72e−7	4.02	1.07e−4	3.01	1.12e−6	4.00
	4096	4.32e−8	3.99	1.32e−5	2.99	8.66e−8	4.00	4.79e−8	4.01	1.33e−5	3.01	7.02e−8	4.00

Table 3
Example 1: History of convergence of the HDG methods for $\omega = 4$.

Degree k	Mesh n_e	HDG-I						HDG-II					
		$\|\boldsymbol{u}-\boldsymbol{u}_h\|_{\mathcal{T}_h}$		$\|\boldsymbol{u}-\boldsymbol{u}_h\|_{\boldsymbol{H}^c}$		$\|\boldsymbol{u}-\boldsymbol{u}_h^*\|_{\boldsymbol{H}^c}$		$\|\boldsymbol{u}-\boldsymbol{u}_h\|_{\mathcal{T}_h}$		$\|\boldsymbol{u}-\boldsymbol{u}_h\|_{\boldsymbol{H}^c}$		$\|\boldsymbol{u}-\boldsymbol{u}_h^*\|_{\boldsymbol{H}^c}$	
		Error	Order	Error	Order	Error	Order	Error	Order	Error	Order	Error	Order
1	16	9.46e−1	–	7.13e−0	–	3.04e−0	–	8.72e−1	–	6.53e−0	–	2.68e−0	–
	64	1.95e−1	2.27	3.27e−0	1.12	7.73e−1	1.98	2.41e−1	1.86	3.43e−0	0.93	6.47e−1	2.05
	256	4.86e−2	2.01	1.65e−0	0.99	1.90e−1	2.02	5.60e−2	2.11	1.69e−0	1.02	1.55e−1	2.06
	1024	1.22e−2	1.99	8.28e−1	0.99	4.75e−2	2.00	1.36e−2	2.04	8.30e−1	1.02	3.83e−2	2.01
	4096	3.07e−3	1.99	4.15e−1	1.00	1.19e−2	2.00	3.36e−3	2.02	4.11e−1	1.01	9.56e−3	2.00
2	16	1.89e−1	–	2.38e−0	–	7.67e−1	–	3.26e−1	–	3.71e−0	–	7.97e−1	–
	64	2.67e−2	2.83	7.11e−1	1.74	9.69e−2	2.99	3.08e−2	3.40	7.93e−1	2.22	8.87e−2	3.17
	256	3.25e−3	3.04	1.73e−1	2.04	1.20e−2	3.02	3.75e−3	3.04	1.90e−1	2.06	1.08e−2	3.04
	1024	3.99e−4	3.03	4.21e−2	2.03	1.49e−3	3.00	4.63e−4	3.02	4.66e−2	2.03	1.35e−3	3.00
	4096	4.92e−5	3.02	1.04e−2	2.02	1.86e−4	3.00	5.74e−5	3.01	1.15e−2	2.02	1.69e−4	3.00
3	16	3.90e−2	–	7.52e−1	–	1.58e−1	–	4.12e−2	–	7.67e−1	–	1.25e−1	–
	64	2.65e−3	3.88	1.00e−1	2.91	1.04e−2	3.92	3.28e−3	3.65	1.13e−1	2.76	8.14e−3	3.94
	256	1.70e−4	3.96	1.30e−2	2.94	6.76e−4	3.94	2.00e−4	4.04	1.40e−2	3.01	5.30e−4	3.94
	1024	1.08e−5	3.97	1.67e−3	2.97	4.27e−5	3.99	1.23e−5	4.02	1.74e−3	3.02	3.33e−5	3.99
	4096	6.84e−7	3.99	2.10e−4	2.99	2.67e−6	4.00	7.67e−7	4.01	2.15e−4	3.01	2.09e−6	4.00

Table 4
Example 1: The condition number ratio R of the global stiffness matrix as a function of k, n_e and ω for the HDG-II method.

Degree k	Mesh n_e	Frequency				
		$\omega = 1$	$\omega = \sqrt{2}$	$\omega = 2$	$\omega = 2\sqrt{2}$	$\omega = 4$
1	64	1.0617	1.0417	1.0120	0.9672	0.8976
	256	1.1361	1.1255	1.1102	1.0879	1.0554
	1024	1.1632	1.1579	1.1503	1.1394	1.1238
2	64	1.0844	1.0730	1.0559	1.0295	0.9911
	256	1.1415	1.1360	1.1279	1.1161	1.0986
	1024	1.1615	1.1588	1.1549	1.1493	1.1412
3	64	0.9689	0.9619	0.9512	0.9347	0.9086
	256	1.0352	1.0316	1.0264	1.0186	1.0070
	1024	1.0556	1.0539	1.0513	1.0476	1.0423

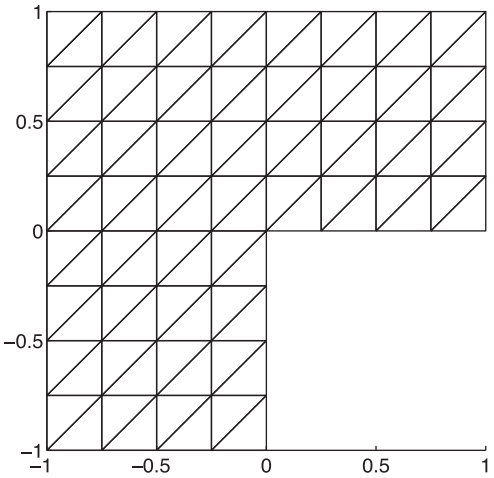

Fig. 3. The initial mesh for the L-shaped domain.

Table 5
Example 2: History of convergence of the HDG methods for $\omega = 6$.

Degree k	Mesh h	HDG-I						HDG-II					
		$\|\boldsymbol{u}-\boldsymbol{u}_h\|_{\mathcal{T}_h}$		$\|\boldsymbol{u}-\boldsymbol{u}_h\|_{\boldsymbol{H}^c}$		$\|\boldsymbol{u}-\boldsymbol{u}_h^*\|_{\boldsymbol{H}^c}$		$\|\boldsymbol{u}-\boldsymbol{u}_h\|_{\mathcal{T}_h}$		$\|\boldsymbol{u}-\boldsymbol{u}_h\|_{\boldsymbol{H}^c}$		$\|\boldsymbol{u}-\boldsymbol{u}_h^*\|_{\boldsymbol{H}^c}$	
		Error	Order	Error	Order	Error	Order	Error	Order	Error	Order	Error	Order
1	1/4	6.48e−1	–	9.44e−0	–	3.90e−0	–	1.12e−0	–	1.45e−9	–	5.82e−0	–
	1/8	9.43e−2	2.78	4.51e−0	1.07	5.5e−1	2.83	2.75e−1	2.03	5.14e−0	1.50	1.59e−0	1.87
	1/16	2.22e−2	2.09	2.28e−0	0.98	1.26e−1	2.13	5.71e−2	2.27	2.34e−0	1.14	3.29e−1	2.28
	1/32	5.58e−3	1.99	1.15e−0	0.99	3.14e−2	2.01	9.25e−3	2.63	1.14e−0	1.03	4.92e−2	2.74
	1/24	1.40e−3	2.00	5.75e−1	1.00	7.82e−3	2.00	1.75e−3	2.40	5.67e−1	1.01	8.27e−3	2.57
2	1/4	1.08e−1	–	2.16e−0	–	6.26e−1	–	1.19e−1	–	2.38e−0	–	6.65e−1	–
	1/8	7.19e−3	3.91	4.87e−1	2.15	3.79e−2	4.05	8.17e−3	3.87	5.46e−1	2.13	3.70e−2	4.17
	1/16	7.51e−4	3.26	1.17e−1	2.06	3.95e−3	3.26	8.88e−4	3.20	1.33e−1	2.04	3.63e−3	3.35
	1/32	9.04e−5	3.06	2.86e−2	2.03	4.88e−4	3.02	1.09e−4	3.03	3.29e−2	2.02	4.45e−4	3.03
	1/64	1.11e−5	3.02	7.10e−3	2.01	6.11e−5	3.00	1.35e−5	3.01	8.17e−3	2.01	5.55e−5	3.00
3	1/4	5.21e−3	–	2.97e−1	–	2.92e−2	–	6.82e−3	–	3.52e−1	–	2.82e−2	–
	1/8	3.37e−4	3.95	3.82e−2	2.96	1.94e−3	3.91	3.92e−4	4.12	4.27e−2	3.05	1.53e−3	4.20
	1/16	2.13e−5	3.99	4.87e−3	2.97	1.21e−4	4.00	2.42e−5	4.02	5.24e−3	3.03	9.55e−5	4.00
	1/32	1.34e−6	3.99	6.14e−4	2.99	7.52e−6	4.01	1.50e−6	4.01	6.48e−4	3.01	5.96e−6	4.00
	1/64	8.38e−8	4.00	7.70e−5	2.99	4.69e−7	4.00	9.36e−8	4.01	8.06e−5	3.01	3.72e−7	4.00

where $f = J_\alpha(\omega r)\cos(\alpha\theta)$ with $r = \sqrt{x^2+y^2}$ and $\theta = \tan^{-1}(y/x)$. Here J_α is the Bessel function of the first kind of order α. We choose $\alpha = 0$ so that the exact solution is smooth.

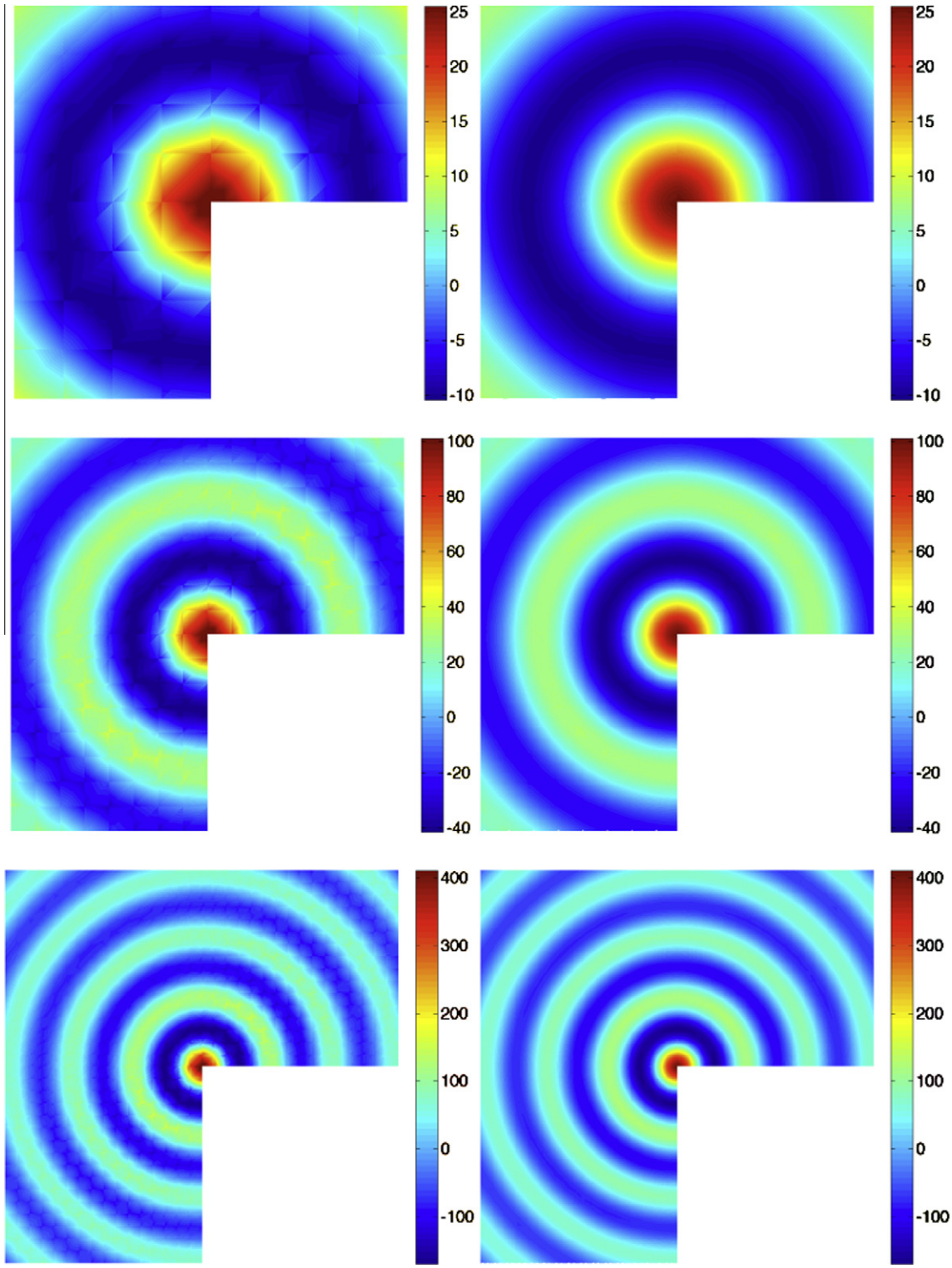

Fig. 4. The plots of $\nabla \times \boldsymbol{u}_h$ (left) and $\nabla \times \boldsymbol{u}_h^*$ (right) for $\omega = 5$ (top), $\omega = 10$ (middle) and $\omega = 20$ (bottom). These results are obtained using $h = 1/8$ (for $\omega = 5$), $h = 1/16$ (for $\omega = 10$) and $h = 1/32$ (for $\omega = 20$) and the same polynomial degree $k = 2$.

We use structured triangular meshes that are refinements of an initial uniform mesh of 96 triangles as shown in Fig. 3. Each refinement is obtained by subdividing every triangle into four smaller triangles. We say that the mesh has refinement

Table 6
Example 2: The condition number ratio R of the global stiffness matrix as a function of k, h and ω for the HDG-II method.

Degree k	Mesh h	Frequency					
		$\omega = 1$	$\omega = \sqrt{2}$	$\omega = 2$	$\omega = 2\sqrt{2}$	$\omega = 4$	$\omega = 4\sqrt{2}$
1	1/4	0.9523	0.9312	1.8896	0.9250	0.8960	2.1259
	1/8	1.0107	1.0002	1.9421	0.9623	0.9301	1.8670
	1/16	1.0319	1.0267	1.9525	1.0085	0.9931	1.8423
	1/32	1.0403	1.0377	1.9547	1.0288	1.0214	1.8392
2	1/4	0.9686	0.9573	1.0106	0.9155	0.8774	0.8538
	1/8	1.0071	1.0017	1.0481	0.9822	0.9652	0.9397
	1/16	1.0206	1.0179	1.0593	1.0086	1.0006	0.9890
	1/32	1.0256	1.0242	1.0630	1.0197	1.0158	1.0103
3	1/4	0.8914	0.8840	0.8727	0.8555	0.8285	0.7850
	1/8	0.9268	0.9233	0.9181	0.9105	0.8990	0.8815
	1/16	0.9380	0.9363	0.9338	0.9303	0.9251	0.9174
	1/32	0.9418	0.9409	0.9397	0.9380	0.9356	0.9320

level ℓ if it is obtained from the initial mesh after we perform ℓ refinements. Since our meshes are regular all elements have the same size $h = 1/2^{\ell+2}$ which is the length of the shortest edge.

We first present in Table 5 the error and order of convergence of both HDG-I and HDG-II for $\omega = 6$. We observe for both HDG-I and HDG-II that $\boldsymbol{u}_h$ converges with order $k+1$ in the L^2-norm and with order k in the $\boldsymbol{H}^{\text{curl}}(\mathcal{T}_h)$-norm. We also see that $\boldsymbol{u}_h^*$ converges with order $k+1$ in the $\boldsymbol{H}^{\text{curl}}(\Omega)$-norm. These results are similar to those of the square domain problem. In order to visualize the effectiveness of the local postprocessing scheme, we show in Fig. 4 the plots of both $\nabla \times \boldsymbol{u}_h$ and $\nabla \times \boldsymbol{u}_h^*$ obtained using HDG-II for $\omega = 5$, 10, and 20. It is clear that $\nabla \times \boldsymbol{u}_h^*$ is superior to $\nabla \times \boldsymbol{u}_h$.

Finally, we report in Table 6 the condition number ratio R as a function of k, h and ω. Here the condition number ratio R is defined as

$$R = \frac{C}{60(3k^{1.4} - 1)(\omega h)^{-2}},$$

where C is the condition number of the stiffness matrix G in (65) of the HDG-II method. We see that the condition number ratio R is close to 1 except for the case $k = 1$ at $\omega = 2$ and $\omega = 4\sqrt{2}$ where it is close to 2. We observe that for the range of frequency considered here the condition number is proportional to $(\omega h)^{-2}$ as k is fixed. It implies that the condition number increases as the frequency ω decreases if we keep both h and k fixed. These results are quite similar to those of the previous example and demonstrate that the HDG-II method is computationally attractive for solving the time-harmonic Maxwell's equations.

7.3. The L-shaped domain problem with nonsmooth solution

We revisit the L-shaped domain problem described above. We follow [1,23] and choose $\alpha = 2/3$ so that the exact solution $\boldsymbol{u}$ resides in the Sobolev space $\boldsymbol{H}^{2/3-\varepsilon}(\Omega)$ for $\varepsilon > 0$. Hence, the exact solution is nonsmooth and indeed singular at the entrant corner (0,0). In this example, we investigate two different types of meshes, namely, uniform meshes described earlier and adaptive meshes shown in Fig. 5. These adaptive meshes are refined toward the entrant corner in order to capture the singularity of the exact solution. A summary of these meshes is listed in Table 7.

We present in Fig. 6 the errors in both the L^2-norm and $\boldsymbol{H}^{\text{curl}}$-norm versus the number of global degrees of freedom N for the HDG-II method. Here N is equal to the dimension of the stiffness matrix G in (65). We make two important observations. First, we observe that the errors in both the L^2-norm and $\boldsymbol{H}^{\text{curl}}$-norm converge to zero at the rate $O(h^{2/3})$ on uniformly refined meshes. Although increasing the polynomial degree k leads to a decrease in the errors, the convergence rate remains $O(h^{2/3})$ regardless of values of k. Our results agree very well with the previous results reported in [1,23] and demonstrate that p-refinement strategy is not effective for problems with singular solutions. Second, we observe that the errors on adaptively refined meshes converge at faster rate and are significantly smaller than those on uniformly refined meshes for the same number of degrees of freedom. This demonstrates that h-refinement strategy is much more effective than p-refinement strategy for this problem.

Finally, we would like to emphasize that our local postprocessing works well for this problem with nonsmooth solution since it improves the accuracy of the approximate solution especially on adaptive meshes. In particular, we observe that $\|\boldsymbol{u} - \boldsymbol{u}_h^*\|_{\boldsymbol{H}^c}$ is several times smaller than $\|\boldsymbol{u} - \boldsymbol{u}_h\|_{\boldsymbol{H}^c}$ for the same mesh and polynomial degree. For instance, for the mesh (c) in Fig. 5 and $k = 1$, we obtain $\|\boldsymbol{u} - \boldsymbol{u}_h\|_{\boldsymbol{H}^c} = 1.09 \times 10^{-2}$ and $\|\boldsymbol{u} - \boldsymbol{u}_h^*\|_{\boldsymbol{H}^c} = 4.76 \times 10^{-4}$. This demonstrates the effectiveness of the local postprocessing, especially when it is combined with h-refinement strategy, for improving the accuracy and convergence rate of the HDG solution.

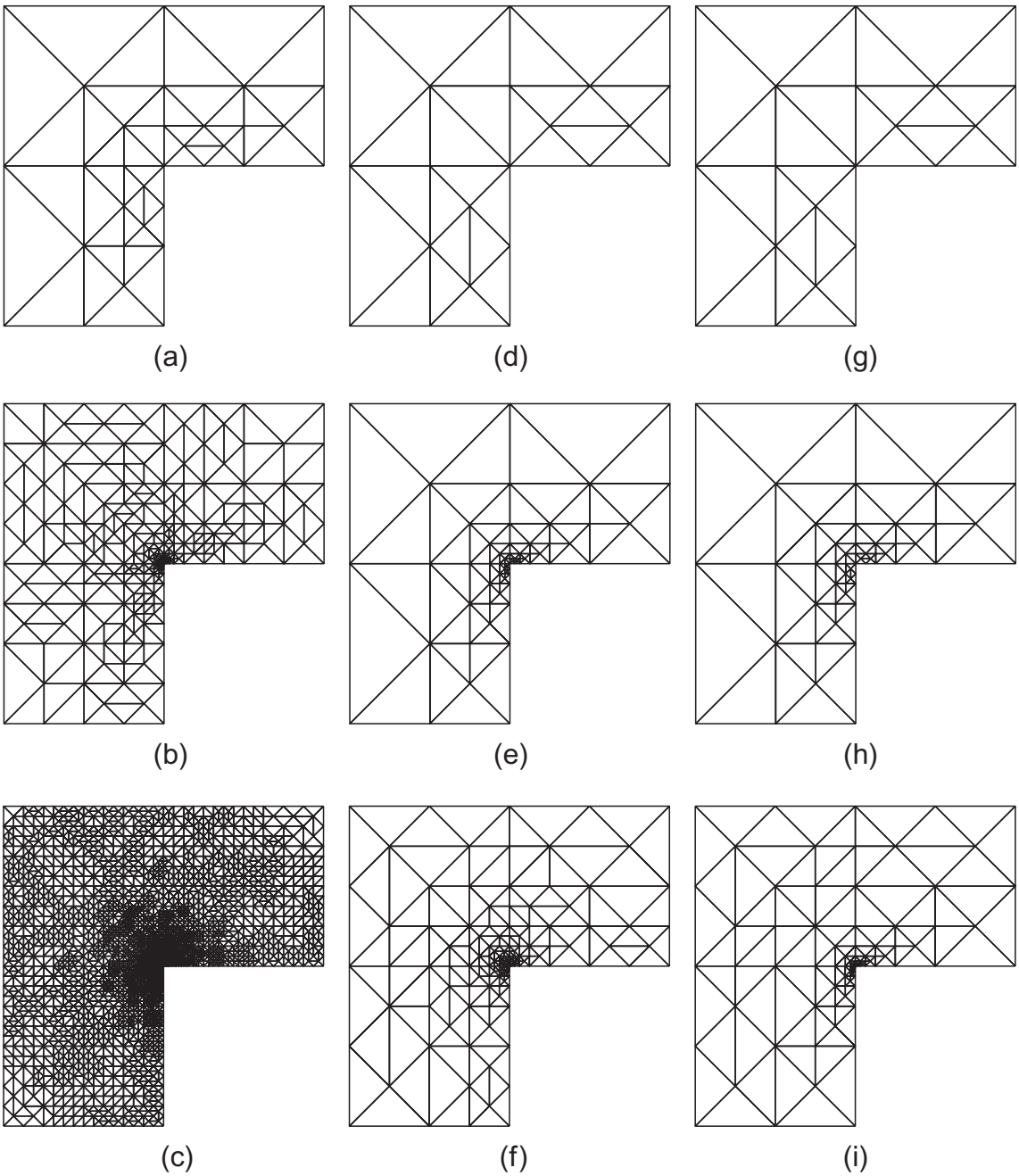

Fig. 5. Example 3: Sequence of adaptive meshes refined toward the entrant corner. The meshes in (a), (b) and (c) are used in computation for $k = 1$. The meshes in (d), (e) and (f) are used in computation for $k = 2$. The meshes in (g), (h) and (i) are used in computation for $k = 3$.

8. Conclusion

We have presented two hybridizable discontinuous Galerkin (HDG) methods for the numerical solution of the time-harmonic Maxwell's equations. The first HDG method is developed for the mixed curl–curl formulation and is named HDG-I, while the second HDG method is developed for the vector wave equation and is named HDG-II. The HDG methods retain the strengths of standard DG methods and have the following advantages:

- The globally coupled unknowns are the approximate trace of the tangential component of the vector field for the HDG-II method and, in the case of the HDG-I method, the approximate trace of the Lagrange multiplier. Since the approximate

Table 7
Example 3: Summary of basic information of the meshes displayed in Fig. 5.

Mesh	# Elements	# Nodes	# Edges	$h_{\min}$	$h_{\max}$
(a)	48	32	79	1.77e−1	1.0
(b)	540	295	834	6.90e−4	0.5
(c)	5746	2971	8716	2.70e−6	0.125
(d)	28	21	48	3.54e−1	1.0
(e)	108	65	172	2.21e−2	1.0
(f)	392	219	610	8.63e−5	0.5
(g)	28	21	48	3.54e−1	1.0
(h)	88	54	141	4.42e−2	1.0
(i)	274	157	430	1.73e−4	0.5

traces are single-valued across the inter-element boundaries, the HDG methods have considerably less globally coupled unknowns than standard DG methods and thus result in significant savings in both the computational time and memory storage.

- The numerical solution can be postprocessed at the element level to yield a new approximate vector field which is $\boldsymbol{H}^{\mathrm{curl}}(\Omega)$-conforming and converges with order $k+1$ in the $\boldsymbol{H}^{\mathrm{curl}}(\Omega)$-norm for problems with smooth solutions. For problems with nonsmooth solutions, the local postprocessing is also effective in improving accuracy especially when it is combined with h-refinement strategy.
- Both the HDG methods perform well for a wide range of frequencies and produce similar convergence rate and accuracy. Therefore, the HDG-II method is a method of choice since its global stiffness matrix is much smaller than that of the HDG-I method. Furthermore, we observe by numerical experiments that for the low range of frequency considered in the numerical examples the condition number of the stiffness matrix of the HDG-II method decreases as the frequency increases. Moreover, the stiffness matrix is compact in the sense that only the degrees of freedom among neighboring elements are connected. These features of the stiffness matrix make the HDG-II method very attractive for iterative solution methods [38].

Finally, we close by pointing out several possible extensions and directions for further research. First, we note that h/p-refinement strategy is a better approach for problems with singular solutions because the correct combination of h- and p-refinements can yield exponential convergence rates, whereas h-refinement can only give algebraic convergence rates [17,18,24]. Therefore, it is natural to extend the current approach to h/p-refinement. Another possibility is the enrichment of the polynomial spaces with non-polynomial basis functions to represent the approximate solution in order to capture singularities and discontinuities. The HDG methods lend themselves very flexible for incorporating non-polynomial functions into the approximation spaces because the enrichment can be done at the local solvers. We would also like to extend the methods to eddy current problems on multiply connected domains [25], Maxwell's eigenvalue problems and time-dependent Maxwell's equations.

Acknowledgments

We would like to thank Mr. Zhang Wujun of UMN for adaptively refined meshes. J. Peraire and N.C. Nguyen would like to acknowledge the Singapore-MIT Alliance and the AFOSR Grant FA9550-08-1-0350 for partially supporting this work. B. Cockburn would like to acknowledge the National Science Foundation for partially supporting this work through Grant DMS-0712955.

Appendix A. Proof of Lemma 3.2

Proof. We first note that the local solvers (24) can be expressed explicitly as follow. The first local solver is given by

$$\begin{aligned}
&(\mu \boldsymbol{w}_h^{\boldsymbol{\eta}}, \boldsymbol{r})_K - (\boldsymbol{u}_h^{\boldsymbol{\eta}}, \nabla \times \boldsymbol{r})_K = \langle \boldsymbol{\eta}, \boldsymbol{r} \times \boldsymbol{n} \rangle_{\partial K},\\
&(\nabla \times \boldsymbol{w}_h^{\boldsymbol{\eta}}, \boldsymbol{v})_K + \langle \tau_t \boldsymbol{u}_h^{\boldsymbol{\eta}} \times \boldsymbol{n}, \boldsymbol{v} \times \boldsymbol{n} \rangle_{\partial K} - (p_h^{\boldsymbol{\eta}}, \nabla \cdot \epsilon \boldsymbol{v})_K - (\epsilon\omega^2 \boldsymbol{u}_h^{\boldsymbol{\eta}}, \boldsymbol{v})_K = \langle \tau_t \boldsymbol{\eta}, \boldsymbol{v} \times \boldsymbol{n} \rangle_{\partial K},\\
&(\nabla \cdot \epsilon \boldsymbol{u}_h^{\boldsymbol{\eta}}, q)_K + \langle \tau_n p_h^{\boldsymbol{\eta}}, \epsilon q \rangle_{\partial K} = 0;
\end{aligned} \tag{A.1}$$

the second local solver is given by

$$\begin{aligned}
&(\mu \boldsymbol{w}_h^{\zeta}, \boldsymbol{r})_K - (\boldsymbol{u}_h^{\zeta}, \nabla \times \boldsymbol{r})_K = 0,\\
&(\nabla \times \boldsymbol{w}_h^{\zeta}, \boldsymbol{v})_K + \langle \tau_t \boldsymbol{u}_h^{\zeta} \times \boldsymbol{n}, \boldsymbol{v} \times \boldsymbol{n} \rangle_{\partial K} - (p_h^{\zeta}, \nabla \cdot \epsilon \boldsymbol{v})_K - (\epsilon\omega^2 \boldsymbol{u}_h^{\zeta}, \boldsymbol{v})_K = -\langle \epsilon\zeta, \boldsymbol{v} \cdot \boldsymbol{n} \rangle_{\partial K},\\
&(\nabla \cdot \epsilon \boldsymbol{u}_h^{\zeta}, q)_K + \langle \tau_n p_h^{\zeta}, \epsilon q \rangle_{\partial K} = \langle \tau_n \zeta, \epsilon q \rangle_{\partial K};
\end{aligned} \tag{A.2}$$

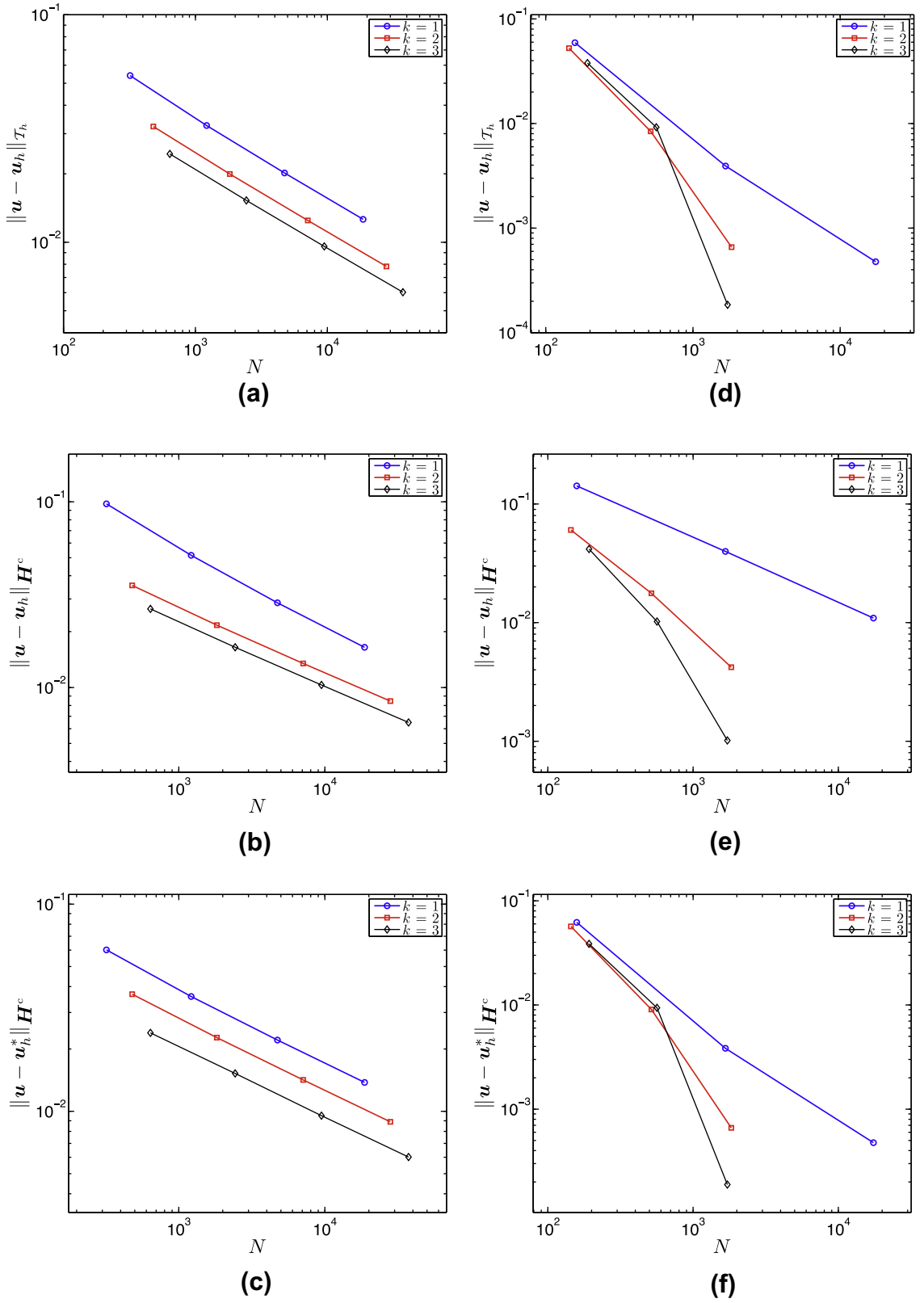

Fig. 6. Example 3: Plots of the errors in the L^2-norm and $\boldsymbol{H}^{\text{curl}}$-norm for uniform meshes (left) and adaptive meshes (right) versus the number of global degrees of freedom N for the HDG-II method. Results in (a), (b) and (c) are obtained on uniformly refined meshes described earlier, while results in (d), (e) and (f) are obtained on adaptively refined meshes displayed in Fig. 5.

and the third local solver is given by

$$\begin{aligned}
&\left(\mu \boldsymbol{w}_h^{\boldsymbol{j}}, \boldsymbol{r}\right)_K - \left(\boldsymbol{u}_h^{\boldsymbol{j}}, \nabla \times \boldsymbol{r}\right)_K = 0,\\
&\left(\nabla \times \boldsymbol{w}_h^{\boldsymbol{j}}, \boldsymbol{v}\right)_K + \left\langle \tau_t \boldsymbol{u}_h^{\boldsymbol{j}} \times \boldsymbol{n}, \boldsymbol{v} \times \boldsymbol{n}\right\rangle_{\partial K} - \left(p_h^{\boldsymbol{j}}, \nabla \cdot \epsilon \boldsymbol{v}\right)_K - \left(\epsilon\omega^2 \boldsymbol{u}_h^{\boldsymbol{j}}, \boldsymbol{v}\right)_K = (\boldsymbol{j}, \boldsymbol{v})_K,\\
&\left(\nabla \cdot \epsilon \boldsymbol{u}_h^{\boldsymbol{j}}, q\right)_K + \left\langle \tau_n p_h^{\boldsymbol{j}}, \epsilon q\right\rangle_{\partial K} = 0.
\end{aligned} \tag{A.3}$$

We use the above local solvers to prove the identities in (28) as follows.

The first identity $I_1 \equiv -\left\langle \boldsymbol{n} \times \boldsymbol{w}_h^{\xi} + \tau_t\left((\boldsymbol{u}_h^t)^{\xi} - \xi\right), \boldsymbol{\eta}\right\rangle_{\partial \mathcal{T}_h}$ can be derived as follows

$$\begin{aligned}
I_1 &= \left(\mu \boldsymbol{w}_h^{\xi}, \boldsymbol{w}_h^{\boldsymbol{\eta}}\right)_{\mathcal{T}_h} - \left(\boldsymbol{u}_h^{\boldsymbol{\eta}}, \nabla \times \boldsymbol{w}_h^{\xi}\right)_{\mathcal{T}_h} - \left\langle \tau_t\left((\boldsymbol{u}_h^t)^{\xi} - \xi\right), \boldsymbol{\eta}\right\rangle_{\partial \mathcal{T}_h}\\
&= \left(\mu \boldsymbol{w}_h^{\xi}, \boldsymbol{w}_h^{\boldsymbol{\eta}}\right)_{\mathcal{T}_h} - \left(p^{\xi}, \nabla \cdot \epsilon \boldsymbol{u}_h^{\boldsymbol{\eta}}\right)_{\mathcal{T}_h} - \left(\epsilon\omega^2 \boldsymbol{u}_h^{\xi}, \boldsymbol{u}_h^{\boldsymbol{\eta}}\right)_{\mathcal{T}_h} + \left\langle \tau_t\left((\boldsymbol{u}_h^t)^{\xi} - \xi\right), (\boldsymbol{u}_h^t)^{\boldsymbol{\eta}} - \boldsymbol{\eta}\right\rangle_{\partial \mathcal{T}_h}\\
&= \left(\mu \boldsymbol{w}_h^{\xi}, \boldsymbol{w}_h^{\boldsymbol{\eta}}\right)_{\mathcal{T}_h} - \left(\epsilon\omega^2 \boldsymbol{u}_h^{\xi}, \boldsymbol{u}_h^{\boldsymbol{\eta}}\right)_{\mathcal{T}_h} + \left\langle \tau_n \epsilon p_h^{\xi}, p_h^{\boldsymbol{\eta}}\right\rangle_{\partial \mathcal{T}_h} + \left\langle \tau_t\left((\boldsymbol{u}_h^t)^{\xi} - \xi\right), (\boldsymbol{u}_h^t)^{\boldsymbol{\eta}} - \boldsymbol{\eta}\right\rangle_{\partial \mathcal{T}_h},
\end{aligned}$$

by the first, second, and third equations of the local solver (A.1), respectively.

For the second identity $I_2 \equiv -\left\langle \boldsymbol{n} \times \boldsymbol{w}_h^{\varrho} + \tau_t (\boldsymbol{u}_h^t)^{\varrho}, \boldsymbol{\eta}\right\rangle_{\partial \mathcal{T}_h}$ we note that

$$I_2 = \left(\mu \boldsymbol{w}_h^{\boldsymbol{\eta}}, \boldsymbol{w}_h^{\varrho}\right)_{\mathcal{T}_h} - \left(\boldsymbol{u}_h^{\boldsymbol{\eta}}, \nabla \times \boldsymbol{w}_h^{\varrho}\right)_{\mathcal{T}_h} - \left\langle \tau_t (\boldsymbol{u}_h^t)^{\varrho}, \boldsymbol{\eta}\right\rangle_{\partial \mathcal{T}_h} = \left(\boldsymbol{u}_h^{\varrho}, \nabla \times \boldsymbol{w}_h^{\boldsymbol{\eta}}\right)_{\mathcal{T}_h} - \left(\boldsymbol{u}_h^{\boldsymbol{\eta}}, \nabla \times \boldsymbol{w}_h^{\varrho}\right)_{\mathcal{T}_h} - \left\langle \tau_t (\boldsymbol{u}_h^t)^{\varrho}, \boldsymbol{\eta}\right\rangle_{\partial \mathcal{T}_h}$$

by the first equation of (A.1) and the first equation of (A.2), respectively. Then we have

$$\begin{aligned}
I_2 &= \left(\epsilon\omega^2 \boldsymbol{u}_h^{\boldsymbol{\eta}}, \boldsymbol{u}_h^{\varrho}\right)_{\mathcal{T}_h} + \left(p_h^{\boldsymbol{\eta}}, \nabla \cdot \epsilon \boldsymbol{u}_h^{\varrho}\right)_{\mathcal{T}_h} - \left\langle \tau_t (\boldsymbol{u}_h^t)^{\boldsymbol{\eta}}, (\boldsymbol{u}_h^t)^{\varrho}\right\rangle_{\partial \mathcal{T}_h} - \left(\boldsymbol{u}_h^{\boldsymbol{\eta}}, \nabla \times \boldsymbol{w}_h^{\varrho}\right)_{\mathcal{T}_h}\\
&= \left(\epsilon\omega^2 \boldsymbol{u}_h^{\boldsymbol{\eta}}, \boldsymbol{u}_h^{\varrho}\right)_{\mathcal{T}_h} - \left\langle \tau_t (\boldsymbol{u}_h^t)^{\boldsymbol{\eta}}, (\boldsymbol{u}_h^t)^{\varrho}\right\rangle_{\partial \mathcal{T}_h} + \left(p_h^{\boldsymbol{\eta}}, \nabla \cdot \epsilon \boldsymbol{u}_h^{\varrho}\right)_{\mathcal{T}_h} - \left(\epsilon\omega^2 \boldsymbol{u}_h^{\boldsymbol{\eta}}, \boldsymbol{u}_h^{\varrho}\right)_{\mathcal{T}_h}\\
&\quad + \left\langle \tau_t (\boldsymbol{u}_h^t)^{\boldsymbol{\eta}}, (\boldsymbol{u}_h^t)^{\varrho}\right\rangle_{\partial \mathcal{T}_h} - \left(p_h^{\varrho}, \nabla \cdot \epsilon \boldsymbol{u}_h^{\boldsymbol{\eta}}\right)_{\mathcal{T}_h} + \left\langle \epsilon \varrho, \boldsymbol{u}_h^{\boldsymbol{\eta}} \cdot \boldsymbol{n}\right\rangle_{\partial \mathcal{T}_h}\\
&= \left\langle \tau_n p_h^{\boldsymbol{\eta}}, \epsilon p_h^{\varrho}\right\rangle_{\partial \mathcal{T}_h} - \left\langle \tau_n p_h^{\boldsymbol{\eta}}, \epsilon p_h^{\varrho}\right\rangle_{\partial \mathcal{T}_h} + \left\langle \tau_n p_h^{\boldsymbol{\eta}}, \epsilon \varrho\right\rangle_{\partial \mathcal{T}_h} + \left\langle \epsilon \varrho, (\boldsymbol{u}_h^{\eta})^{\boldsymbol{\eta}} \cdot \boldsymbol{n}\right\rangle_{\partial \mathcal{T}_h}
\end{aligned}$$

by the second equation of (A.1), the second equation of (A.2), and the third equation of (A.1) and (A.3), respectively.

For the third identity $I_3 \equiv -\left\langle \boldsymbol{n} \times \boldsymbol{w}_h^{\boldsymbol{j}} + \tau_t (\boldsymbol{u}_h^t)^{\boldsymbol{j}}, \boldsymbol{\eta}\right\rangle_{\partial \mathcal{T}_h}$ we note that

$$I_3 = \left(\mu \boldsymbol{w}_h^{\boldsymbol{\eta}}, \boldsymbol{w}_h^{\boldsymbol{j}}\right)_{\mathcal{T}_h} - \left(\boldsymbol{u}_h^{\boldsymbol{\eta}}, \nabla \times \boldsymbol{w}_h^{\boldsymbol{j}}\right)_{\mathcal{T}_h} - \left\langle \tau_t (\boldsymbol{u}_h^t)^{\boldsymbol{j}}, \boldsymbol{\eta}\right\rangle_{\partial \mathcal{T}_h} = \left(\boldsymbol{u}_h^{\boldsymbol{j}}, \nabla \times \boldsymbol{w}_h^{\boldsymbol{\eta}}\right)_{\mathcal{T}_h} - \left(\boldsymbol{u}_h^{\boldsymbol{\eta}}, \nabla \times \boldsymbol{w}_h^{\boldsymbol{j}}\right)_{\mathcal{T}_h} - \left\langle \tau_t (\boldsymbol{u}_h^t)^{\boldsymbol{j}}, \boldsymbol{\eta}\right\rangle_{\partial \mathcal{T}_h}$$

by the first equation of (A.1) and the first equation of (A.3), respectively. Then we have

$$\begin{aligned}
I_3 &= \left(\epsilon\omega^2 \boldsymbol{u}_h^{\boldsymbol{\eta}}, \boldsymbol{u}_h^{\boldsymbol{j}}\right)_{\mathcal{T}_h} + \left(p_h^{\boldsymbol{\eta}}, \nabla \cdot \epsilon \boldsymbol{u}_h^{\boldsymbol{j}}\right)_{\mathcal{T}_h} - \left\langle \tau_t (\boldsymbol{u}_h^t)^{\boldsymbol{\eta}}, (\boldsymbol{u}_h^t)^{\boldsymbol{j}}\right\rangle_{\partial \mathcal{T}_h} - \left(\boldsymbol{u}_h^{\boldsymbol{\eta}}, \nabla \times \boldsymbol{w}_h^{\boldsymbol{j}}\right)_{\mathcal{T}_h}\\
&= \left(\epsilon\omega^2 \boldsymbol{u}_h^{\boldsymbol{\eta}}, \boldsymbol{u}_h^{\boldsymbol{j}}\right)_{\mathcal{T}_h} - \left\langle \tau_t (\boldsymbol{u}_h^t)^{\boldsymbol{\eta}}, (\boldsymbol{u}_h^t)^{\boldsymbol{j}}\right\rangle_{\partial \mathcal{T}_h} + \left(p_h^{\boldsymbol{\eta}}, \nabla \cdot \epsilon \boldsymbol{u}_h^{\boldsymbol{j}}\right)_{\mathcal{T}_h} - \left(\epsilon\omega^2 \boldsymbol{u}_h^{\boldsymbol{\eta}}, \boldsymbol{u}_h^{\boldsymbol{j}}\right)_{\mathcal{T}_h}\\
&\quad + \left\langle \tau_t (\boldsymbol{u}_h^t)^{\boldsymbol{\eta}}, (\boldsymbol{u}_h^t)^{\boldsymbol{j}}\right\rangle_{\partial \mathcal{T}_h} - \left(p_h^{\boldsymbol{j}}, \nabla \cdot \epsilon \boldsymbol{u}_h^{\boldsymbol{\eta}}\right)_{\mathcal{T}_h} - (\boldsymbol{j}, \boldsymbol{u}_h^{\boldsymbol{\eta}})_{\mathcal{T}_h}\\
&= \left\langle \tau_n p_h^{\boldsymbol{\eta}}, \epsilon p_h^{\boldsymbol{j}}\right\rangle_{\partial K} - \left\langle \tau_n p_h^{\boldsymbol{\eta}}, \epsilon p_h^{\boldsymbol{j}}\right\rangle_{\partial K} - (\boldsymbol{j}, \boldsymbol{u}_h^{\boldsymbol{\eta}})_{\mathcal{T}_h}
\end{aligned}$$

by the second equation of (A.1), the second equation of (A.3), and the third equation of (A.1) and (A.3), respectively.

The last three identities in (29) can be easily derived in a similar manner. This completes the proof. □

References

[1] M. Ainsworth, J. Coyle, Hierarchic *hp*-edge element families for Maxwell's equations on hybrid quadrilateral/triangular meshes, Comput. Methods Appl. Mech. Eng. 190 (2001) 6709–6733.
[2] M. Ainsworth, J. Coyle, Hierarchic finite element bases on unstructured tetrahedral meshes, Int. J. Numer. Methods Eng. 58 (2003) 2103–2130.
[3] D.N. Arnold, F. Brezzi, B. Cockburn, L.D. Marini, Unified analysis of discontinuous Galerkin methods for elliptic problems, SIAM J. Numer. Anal. 39 (2001) 1749–1779.
[4] A. Bossavit, A rationale for 'edge-elements' in 3-D fields computations, IEEE Trans. Magn. 24 (1) (1988) 74–79.
[5] A. Bossavit, Solving maxwell equations in a closed cavity, and the question of 'spurious modes', IEEE Trans. Magn. 26 (2) (1990) 702–705.
[6] B. Cockburn, B. Dong, J. Guzmán, A superconvergent LDG-hybridizable Galerkin method for second-order elliptic problems, Math. Comput. 32 (2) (2007) 233–262.
[7] B. Cockburn, B. Dong, J. Guzmán, M. Restelli, R. Sacco, Superconvergent and optimally convergent LDG-hybridizable discontinuous Galerkin methods for convection–diffusion–reaction problems, SIAM J. Sci. Comput. 31 (2009) 3827–3846.

[8] B. Cockburn, J. Gopalakrishnan, Incompressible finite elements via hybridization. Part I: The Stokes system in two space dimensions, SIAM J. Numer. Anal. 43 (4) (2005) 1627–1650.
[9] B. Cockburn, J. Gopalakrishnan, Incompressible finite elements via hybridization. Part II: The Stokes system in three space dimensions, SIAM J. Numer. Anal. 43 (4) (2005) 1651–1672.
[10] B. Cockburn, J. Gopalakrishnan, The derivation of hybridizable discontinuous Galerkin methods for Stokes flow, SIAM J. Numer. Anal. 47 (2009) 1092–1125.
[11] B. Cockburn, J. Gopalakrishnan, R. Lazarov, Unified hybridization of discontinuous Galerkin, mixed and continuous Galerkin methods for second order elliptic problems, SIAM J. Numer. Anal. 47 (2009) 1319–1365.
[12] B. Cockburn, J. Gopalakrishnan, N.C. Nguyen, J. Peraire, F.-J. Sayas, Analysis of HDG methods for Stokes flow, Math. Comput. 80 (2011) 723–760.
[13] B. Cockburn, J. Gopalakrishnan, F.-J. Sayas, A projection-based error analysis of HDG methods, Math. Comput. 79 (2010) 1351–1367.
[14] B. Cockburn, J. Guzmán, H. Wang, Superconvergent discontinuous Galerkin methods for second-order elliptic problems, Math. Comput. 78 (2009) 1–24.
[15] B. Cockburn, F. Li, C.-W. Shu, Locally divergence-free discontinuous Galerkin methods for the Maxwell equations, J. Comput. Phys. 194 (2) (2004) 588–610.
[16] B. Cockburn, N.C. Nguyen, J. Peraire, A comparison of HDG methods for Stokes flow, J. Sci. Comput. 45 (2010) 215–237.
[17] L. Demkowicz, Computing with *hp*-adaptive finite elements, One and Two Dimensional Elliptic and Maxwell Problems, vol. 1, Chapman and Hall, 2006.
[18] L. Demkowicz, J. Kurtz, D. Pardo, M. Paszynskito, W. Rachowicz, A. Zdunek, Computing with *hp*-adaptive finite elements, Frontiers: Three Dimensional Elliptic and Maxwell Problems with Applications, vol. 2, Chapman and Hall, 2007.
[19] L. Demkowicz, L. Vardapetyan, Modeling of electromagnetic absorption/scattering problems using *hp*-adaptive finite elements, Comput. Methods Appl. Mech. Eng. 152 (1-2) (1998) 103–124.
[20] R.D. Graglia, D.R. Wilton, A.F. Peterson, Higher order interpolatory vector bases for computational electromagnetics, IEEE Trans. Antenna Propagat. 45 (3) (1997) 329–342.
[21] J.S. Hesthaven, T. Warburton, Nodal high-order methods on unstructured grids I. Time-domain solution of Maxwell's equations, J. Comput. Phys. 181 (1) (2002) 186–221.
[22] J.S. Hesthaven, T. Warburton, High-order nodal discontinuous Galerkin methods for the Maxwell eigenvalue problem, Philos. Trans. Roy. Soc. London Ser A: Math. Phys. Eng. Sci. 362 (1816) (2004) 493–524.
[23] P. Houston, I. Perugia, A. Schneebeli, D. Schötzau, Interior penalty method for the indefinite time-harmonic Maxwell equations, Numer. Math. 100 (3) (2005) 485–518.
[24] P.D. Ledger, K. Morgan, The application of the *hp*–finite element method to electromagnetic problems, Arch. Comput. Methods Eng. 12 (3) (2005) 235–302.
[25] P.D. Ledger, S. Zaglmayr, *hp*-Finite element simulation of three-dimensional eddy current problems on multiply connected domains, Comput. Methods Appl. Mech. Eng. 12 (3) (2010) 235–302.
[26] P. Monk, Finite Element Methods for Maxwell's Equations, Clarendon Press, Oxford, 2003.
[27] J.C. Nédélec, Mixed finite elements in R^3, Numer. Math. 35 (3) (1980) 315–341.
[28] J.-C. Nédélec, A new family of mixed finite elements in $\boldsymbol{R}^3$, Numer. Math. 50 (1986) 57–81.
[29] N.C. Nguyen, J. Peraire, B. Cockburn, An implicit high-order hybridizable discontinuous Galerkin method for linear convection–diffusion equations, J. Comput. Phys. 228 (2009) 3232–3254.
[30] N.C. Nguyen, J. Peraire, B. Cockburn, An implicit high-order hybridizable discontinuous Galerkin method for nonlinear convection–diffusion equations, J. Comput. Phys. 228 (2009) 8841–8855.
[31] N.C. Nguyen, J. Peraire, B. Cockburn, A hybridizable discontinuous Galerkin method for Stokes flow, Comput. Methods Appl. Mech. Eng. 199 (2010) 582–597.
[32] N.C. Nguyen, J. Peraire, B. Cockburn, An implicit high-order hybridizable discontinuous Galerkin method the incompressible Navier–Stokes equations, J. Comput. Phys. 230 (2011) 1147–1170.
[33] N.C. Nguyen, J. Peraire, B. Cockburn, Hybridizable discontinuous Galerkin methods, in: Proceedings of the International Conference on Spectral and High Order Methods, Trondheim, Norway, June 2009, Lecture Notes in Computational Science and Engineering, vol. 76, 2011, pp. 63–84.
[34] N.C. Nguyen, J. Peraire, B. Cockburn, A hybridizable discontinuous Galerkin method for the incompressible Navier–Stokes equations (AIAA Paper 2010-362), in: Proceedings of the 48th AIAA Aerospace Sciences Meeting and Exhibit, Orlando, Florida, January 2010.
[35] N.C. Nguyen, J. Peraire, B. Cockburn, HDG methods for acoustics and elastodynamics: superconvergence and postprocessing, J. Comput. Phys. 230 (2011) 3695–3718.
[36] J. Peraire, N.C. Nguyen, B. Cockburn, A hybridizable discontinuous Galerkin method for the compressible Euler and Navier–Stokes equations (AIAA Paper 2010-363), in: Proceedings of the 48th AIAA Aerospace Sciences Meeting and Exhibit, Orlando, Florida, January 2010.
[37] J. Peraire, P.-O. Persson, The compact discontinuous Galerkin (CDG) method for elliptic problems, SIAM J. Sci. Comput. 30 (4) (2008) 1806–1824.
[38] P.O. Persson, J. Peraire, Newton-GMRES preconditioning for discontinuous Galerkin discretizations of the Navier–Stokes equations, SIAM J. Sci. Comput. 30 (6) (2008) 2709–2733.
[39] I. Perugia, D. Schötzau, The *hp*-local discontinuous Galerkin method for low-frequency time-harmonic Maxwell equations, Math. Comput. 72 (243) (2003) 1179–1214.
[40] D. Sármány, M.A. Botchev, J.J. Vegt, Dispersion and dissipation error in high-order Runge–Kutta discontinuous Galerkin discretisations of the Maxwell equations, J. Sci. Comput. 33 (1) (2007) 47–74.
[41] J. Schöberl, S. Zaglamyr, High order Nedelec elements with local complete sequence properties, Int. J. Comput. Math. Electr. Electron. Eng. 24 (2) (2005) 374–384.
[42] R. Sevilla, P.D. Ledger, A comparison of two PMLs for electromagnetic scattering problems in the time domain using high order DG methods, Comput. Methods Appl. Mech. Eng., submitted for publication.
[43] J.P. Webb, Hierarchal vector basis functions of arbitrary order for triangular and tetrahedral finite elements, IEEE Trans. Antenna Propagat. 47 (8) (1999) 1244–1253.
[44] H. Whitney, Geometric Integration Theory, Princeton University Press, 1957.